Bifurcation diagram and a qualitative analysis of particle motion in a Kerr metric

Ivan Bizyaev[*] and Ivan Mamaev[†]

Ural Mathematical Center, Udmurt State University, Universitetskaya 1, Izhevsk 426034, Russia

(Received 16 December 2021; accepted 2 February 2022; published 4 March 2022)

We investigate the dynamics of particles in a Kerr metric which describes the gravitational field in a neighborhood of a rotating black hole. After elimination of cyclic coordinates this problem reduces to investigating a Hamiltonian system with 2 degrees of freedom. This system possesses an additional Carter integral quadratic in momenta and hence is integrable by the Liouville-Arnold theorem. A bifurcation diagram is constructed and a classification of the types of trajectories of the system is carried out according to the values of first integrals. In particular, it is shown that there are seven different regions of values of first integrals which differ in the topological type of the integral submanifold. Pro-and-retrograde trajectories of particles are found.

DOI: 10.1103/PhysRevD.105.063003

I. INTRODUCTION

In a well-known work [1], Smale proposed a topological approach to analysis of dynamical systems which is based on the analysis of the types of integral submanifolds and their bifurcations under changes of first integrals. This approach turned out to be particularly efficient in investigating integrable (and not only Hamiltonian) systems and was used afterward on several occasions in various problems of celestial mechanics [2–4], rigid body dynamics [5–7], vortex dynamics [8,9], etc. This method was further developed in different ways: for example, in Ref. [10,11] possible bifurcations of integral submanifolds were investigated and topological invariants of integrable systems were constructed, whereas the focus of Ref. [4,12] was on the analysis of partial solutions and their stability.

A central role in the topological approach is played by the *bifurcation diagram* of the system, which shows *bifurcation surfaces* (or *curves*) in the space of values of first integrals which correspond to their critical values. It is when these surfaces intersect that the type of the integral submanifolds of the system changes. Furthermore, the critical values of the first integrals correspond to singular partial solutions (critical solutions), which persist under perturbations, including nonintegrable ones (see, e.g., Ref. [13]).

It should be noted that a bifurcation diagram is of fundamental importance to the qualitative analysis of fairly complex integrable systems. In particular, it serves as a basis both in constructing topological invariants and in the stability analysis. In addition, a bifurcation diagram (provided with suitable data on invariant submanifolds) is very illustrative when it comes to a qualitative analysis (see Ref. [4] for details). That is why in this paper we systematically apply this approach to an analysis of the motion of material bodies in a gravitational field given by a Kerr metric.

We also note that, in analyzing the stability of various partial solutions, it is important to keep in mind that in fairly complex systems the stability criteria are obtained, as a rule, in the form of bulky multiparameter inequalities. Therefore, in such cases it is important not only to obtain relations defining the (linear or nonlinear) stability but also to present the results obtained in a comprehensible form, one that allows a comparison to be made with the well-known results and provides a clear understanding of the physical reasons why the stability is lost/acquired, etc. One such approach based on the study of bifurcation diagrams is developed in Ref. [4].

Remark 1.—Figuratively speaking, the role of a bifurcation diagram in analyzing an integrable system is similar to that of a geographic map in exploring a new territory. Of course, in the case of idealized systems (the Kepler problem, a harmonic oscillator, etc.) this diagram is extremely simple and contributes very little to the understanding of the dynamics, whereas for complex systems (the problem of two centers, the Kovalevskaya top, etc.) this diagram can *greatly* facilitate an understanding of the structure of phase space and the analysis of possible types of motion.

Integrability of the geodesic flow in a Kerr metric was established by Carter [14] in 1968, and a large number of results have been obtained since then regarding this problem; see, e.g., the reviews [15–17]. Nevertheless, no complete bifurcation diagram of the system has been constructed thus far, and hence no analysis is available of possible

[*]bizyaevtheory@gmail.com
[†]mamaev@rcd.ru

bifurcations of various types of trajectories of the system under changes of its parameters. Moreover, there is in fact no graphical representation of possible types of motion depending on the values of the first integrals, and, in particular, of the existence and stability of critical trajectories.

At the same time, there are a number of particular results in this direction. For example, bifurcation curves for plane orbits were obtained for the critical value of the Carter integral $Q = 0$ in Ref. [18] [in particular, r_{ISCO} (where the subscript refers to the innermost stable circular orbit) was found for the Kerr metric], and a corresponding diagram was constructed in Ref. [15]. Qualitative analyses of latitudinal motion (i.e., of evolution of the angle θ) were carried out in Ref. [19,20].

Critical spherical orbits (more precisely, spheroidal orbits with $r = \mathrm{const}$) for $a = 1$ were investigated in Ref. [21]. An analysis of spherical orbits for arbitrary a was carried out, for example, in Ref. [22]. The existence of motions of particles with negative energy was first shown in Ref. [23] (see also [24]) in an analysis of the boundary of possible values of energy E and momentum L inside an ergosphere. We note that this boundary also corresponds to the critical values of the integrals (for more details on the case of nonlocal bifurcation, see Sec. III D).

In Ref. [25,26], resonant tori have been found which are filled with noncritical solutions periodic in the reduced system. The solution for the separatrix in the case of planar motion (with $Q = 0$) was found in Ref. [27], and the one in the general case in Ref. [28,29].

Mention should also be made of Ref. [30], in which some bifurcation diagrams are constructed for particle motion in the Kerr-Newman system. However, Ref. [30] ignored physically admissible domains of variation of the variables (for example, r can take negative values) and of the integrals of motion, and therefore it is impossible to understand which of the results have a physical meaning and which of them are purely mathematical in nature.

There are many other papers describing various special properties of (timelike) geodesics of the Kerr metric. We mention some of them which are related to our analysis. For example, in Ref. [31] the motion of particles falling from the state of rest was examined, and Goldstein [32] numerically found trajectories making a large number of turns in the neighborhood of a black hole and then receding from it (see also [33], where such orbits are called "zoom-whirl" orbits). In Ref. [34], a classification of orbits lying on the integral submanifold of the zero angular momentum ($L = 0$) was given.

The paper is structured as follows. In Sec. II we present a Kerr metric in the Boyer-Lindquist coordinates and show that in the Newtonian limit (i.e., if $\frac{|v|}{c} \ll 1$, where v is the velocity of a particle) the problem regarding the motion of a particle reduces to that of a point moving in the potential field of two fixed gravitational centers "located at imaginary points":

$$U = \frac{Gm}{2\sqrt{x^2 + y^2 + (z + ia)^2}} + \frac{Gm}{2\sqrt{x^2 + y^2 + (z - ia)^2}}.$$

In other words, this is a special case of the Euler problem. In addition, we show that outside the horizon the time of a distant observer grows monotonically on timelike geodesics.

Then we write the equations of motion in Hamiltonian form, present the integrals of motion of the system, and obtain a solution in terms of quadratures using the method of separation of variables. We also analyze possible values of Noether's first integrals of energy E and momentum L and show:

(a) if the particle moves outside the ergosphere, then

$$E > 0,$$

(b) if the particle moves inside the ergosphere, then

$$E > E_{\min}(L) = \frac{a}{2(1 + \sqrt{1 - a^2})} L.$$

Moreover, using the Routh reduction, we reduce the analysis of the system to an analysis of a *natural Hamiltonian system with 2 degrees of freedom*.

Section III is concerned with constructing a bifurcation diagram of the (reduced) system and with proving its completeness, i.e., the absence of other critical solutions and corresponding bifurcations of the integral submanifolds. Thereby we find all possible types of integral submanifolds and their bifurcations. In the course of analysis, we find all critical solutions and investigate their stability.

In Sec. IV, based on the results obtained, we carry out a fairly complete analysis of the plane and spherical trajectories of a particle in a Kerr metric.

II. THE MOTION OF PARTICLES IN A KERR METRIC

A Kerr metric is a stationary and cylindrically symmetric solution of the Einstein equations in a vacuum. In particular, it describes the gravitational field of a rotating *black hole*, with no external electromagnetic field present. If the size of a celestial body is larger than the Schwarzschild radius r_s, then for a certain set of multipole moments the gravitational field outside it is also described using the Kerr solution (see [35] for details). Specific examples of such bodies are discussed in Ref. [36,37].

In this section we briefly consider some properties of the Kerr metric [38] and of its geodesics, which we will need in what follows. A more detailed discussion of the physical properties of this metric can be found, for example, in Ref. [14,39,40].

A. The Kerr metric and the Euler problem

1. Limit properties of the Kerr metric

In the Boyer-Lindquist coordinates $\boldsymbol{x} = (t, r, \theta, \varphi)$ the Kerr metric is represented in the following form Ref. [41]:

$$ds^2 = g_{\alpha\beta}dx^\alpha dx^\beta = \frac{\Delta(r)}{\rho^2}(dt - a\sin^2\theta d\varphi)^2 - \frac{\sin^2\theta}{\rho^2}((r^2+a^2)d\varphi - adt)^2 - \rho^2\left(\frac{dr^2}{\Delta(r)} + d\theta^2\right),$$
$$\rho^2 = r^2 + a^2\cos^2\theta, \qquad \Delta(r) = r^2 - 2r + a^2, \tag{1}$$

where an α, $\beta = 0$, 1, 2, 3 summation is implied over repeated indices and the signature (1,3) has been chosen.

In the Kerr metric (1) the coordinates r and t are measured in the following units:

$$\frac{Gm}{c^2}, \qquad \frac{Gm}{c^3},$$

where G is the gravitational constant, c is the velocity of light, and m is the mass of the celestial body (in the chosen units of measurement, $r_s = 2$). The variables $\theta \in (0, \pi)$, $\varphi \in [0, 2\pi)$ are angle variables. The length of the interval is the same as the proper time of the freely moving material point: $ds = d\tau$.

The dimensionless parameter a is expressed in terms of the angular momentum of the celestial body M_z relative to the symmetry axis as follows:

$$a = \frac{cM_z}{Gm^2}.$$

If $a = 0$ (i.e., if there is no rotation), the metric (1) becomes a Schwarzschild metric. A detailed analysis of the trajectory of a material point in this case is carried out, for example, in Ref. [42]. With a suitable choice of the direction of the axis (of rotation), one can always achieve $M_z > 0$, so we assume in what follows that $a > 0$.

For large distances, i.e., for $r \gg 1$ and any values of the parameter a, the metric (1) becomes the following flat Minkowski metric:

$$ds^2 = dt^2 - \rho^2\left(\frac{dr^2}{r^2+a^2} + d\theta^2\right) - (r^2+a^2)\sin^2\theta d\varphi^2 = dt^2 - dx^2 - dy^2 - dz^2, \tag{2}$$

where the Cartesian coordinates are given by the following relations:

$$x = \sqrt{r^2+a^2}\sin\theta\cos\varphi, \qquad y = \sqrt{r^2+a^2}\sin\theta\sin\varphi, \qquad z = r\cos\theta. \tag{3}$$

As can be seen, for Eq. (2) the level surfaces of the *radial coordinate* $r = \text{const}$ with $t = \text{const}$ are confocal spheroids in the three-dimensional Euclidean space

$$\frac{x^2+y^2}{r^2+a^2} + \frac{z^2}{r^2} = 1. \tag{4}$$

The variables θ and φ are *polar* and *azimuthal angles*, respectively, and the coordinate t plays the role of the *time* of an external fixed observer.

We now consider the classical limit of the metric and the first post-Newtonian correction for particle motion with small velocities ($\frac{|v|}{c} \ll 1$). To do so, we make in Eq. (1) the substitution

$$t \to \frac{c^3}{Gm}t, \quad r \to \frac{c^2}{Gm}r, \quad \theta \to \theta, \quad \varphi \to \varphi, \quad a \to \frac{c^2}{Gm}a$$

and define the Lagrangian function of the particle of unit mass as follows, $L = -\frac{Gm}{c^4}\frac{ds}{dt}$, and expand it in powers of c:

$$L = -c^2 + L_0 + \frac{1}{c}L_1 + O\left(\frac{1}{c^2}\right),$$
$$L_0 = \frac{1}{2}\left(\frac{\rho^2}{r^2+a^2}\dot{r}^2 + \rho^2\dot{\theta}^2 + (r^2+a^2)\sin^2\theta\dot{\varphi}^2\right) + \frac{Gmr}{\rho^2},$$
$$L_1 = -2Gma\frac{r\sin^2\theta}{\rho^2}\dot{\varphi},$$

where $\dot{r}$, $\dot{\theta}$, and $\dot{\varphi}$ denote the derivatives with respect to t. Passing to the Cartesian coordinates (3) and neglecting the constant term $(-c^2)$ and terms of order c^{-1}, we represent the resulting Lagrangian in the form

$$L_0 = \frac{1}{2}(\dot{x}^2 + \dot{y}^2 + \dot{z}^2) - U,$$
$$U = \frac{Gm}{2\sqrt{x^2+y^2+(z+ia)^2}} + \frac{Gm}{2\sqrt{x^2+y^2+(z-ia)^2}} = \frac{Gmr}{\rho^2}. \tag{5}$$

Thus, we see that in the classical approximation we obtain a system describing the motion of a particle in the potential of two Newtonian centers (the Euler problem) spaced apart at an "imaginary distance." In this case, the problems regarding particle motion in the Kerr metric and in the Euler system admit separation of variables in the same coordinates [43] (see Sec. II B for details).

Remark 2.—The problem regarding the planar motion of a particle in the field of two fixed Newtonian centers was investigated and reduced to quadratures by Euler

[44,45]. Darboux [46] considered a generalization of the planar Euler problem by adding two complex conjugate masses spaced apart at an imaginary distance. In this case, the potential always takes real values, and the solution to the problem also reduces to quadratures. In addition, the problem regarding the spatial motion of a material point in the field of two Newtonian centers spaced apart at an imaginary distance is a good approximation to the problem regarding a particle (satellite) moving in the field of a flattened spheroid [47,48].

According to relations (4) and (6), the potential U has a singularity on the flat disk

$$z = 0, \qquad x^2 + y^2 \le a^2.$$

The first correction L_1 describes gyroscopic forces (an analog of the magnetic field) whose values are also proportional to the potential U, but, in contrast to Eq. (6), this correction cannot be expressed in a simple form in terms of the coordinates (3).

2. Event horizon and ergosphere

As is well known, an important property of the Boyer-Lindquist coordinates is that for them the surface defining an *event horizon* can be represented in the particularly simple form

$$\mathcal{S}_h = \{(t, r, \theta, \varphi) | r = r_+\} \simeq \mathbb{R} \times \mathbb{S}^2,$$
$$r_+ = 1 + \sqrt{1 - a^2}, \tag{6}$$

where r_+ is the largest root of the equation $\Delta(r) = 0$. According to Eq. (6), for an event horizon to exist, the value of r_+ must be real. This leads to the condition

$$a \le 1.$$

Remark 3.—We note that, by virtue of the inequality $a < 1$, we have $\frac{a}{r} \to_{r\to\infty} 0$ and, generally speaking, relations (2) and (3) with $a \neq 0$ have only a formal mathematical meaning.

From a geometrical point of view, the horizon $\mathcal{S}_h$ determines an isotropic hypersurface [39] (null hypersurface) in spacetime whose section $\mathcal{S}_h^t$ is, for an external observer, diffeomorphic to the two-dimensional sphere $\mathbb{S}^2$ at any instant of time $t = \text{const}$ [since the Kerr metric in the Boyer-Lindquist coordinates (1) is stationary in these variables, the sphere $\mathcal{S}_h^t$ does not depend on t]. In addition, for each point at the event horizon $\mathcal{S}_h$ the light cone (from the region of the future) lies entirely in the region $r \le r_+$, and hence the world lines both of particles and of light beams will, after reaching $r = r_+$, no longer be able to return to the region $r > r_+$ [49].

Since the region $r \le r_+$ turns out to be inaccessible to the external observer, we will consider throughout only the motion of particles outside the event horizon of the Kerr metric (1), i.e., on the manifold

$$\mathcal{N}^4 = \{(t, r, \theta, \varphi) | t \in (-\infty, +\infty), \qquad r \in (r_+, +\infty),$$
$$\theta \in (0, \pi), \qquad \varphi \in [0, 2\pi)\} \simeq \mathbb{R} \times (\mathbb{R}^3 \backslash \mathcal{B}),$$

where the three-dimensional region inside the event horizon in the space is denoted by $\mathcal{B} = \{(r, \theta, \varphi) | r \le r_+\}$.

An important feature of the Kerr solution is the existence of an *ergosphere*. We recall that an ergosphere is a region of space in which any material particle (body) cannot remain at rest relative to any observer for whom the metric is stationary [i.e., $g_{\alpha\beta}(\boldsymbol{x})$ do not depend on x^0]. For example, substituting $dx^1 = 0$, $dx^2 = 0$, and $dx^3 = 0$ into the relation $ds^2 > 0$, which must be satisfied for any world line of material particles, we obtain the condition

$$g_{00}(x^1, x^2, x^3) > 0.$$

This is a condition that must be satisfied by the spatial coordinates x^1, x^2, and x^3 of the points where the particle can be at rest. (It is easy to show that this condition is invariant under changes of variables preserving the stationarity of the metric.) The boundary of this region is defined by the equation

$$g_{00}(x^1, x^2, x^3) = 0$$

and is called the *static surface* $\mathcal{S}_e$.

Accordingly, for the Kerr metric in the Boyer-Lindquist coordinates we find a static surface in the form

$$\mathcal{S}_e = \{(r, \theta, \varphi) | r^2 - 2r + a^2 \cos^2\theta = 0\}.$$

This surface in three-dimensional space lies everywhere outside the event horizon ($r = r_+$) and touches it at two points: $\theta = 0$ and $\theta = \pi$ (see Fig. 1). Therefore, in this case an ergosphere is a region given by the relations

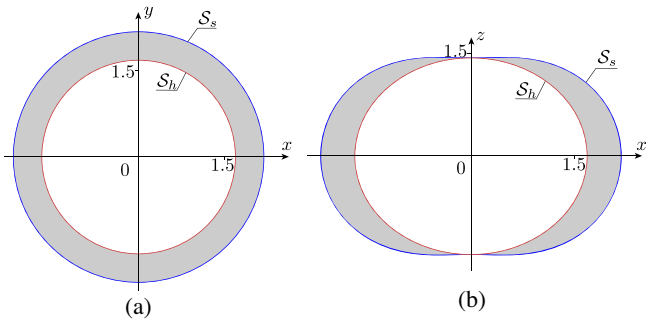

FIG. 1. Typical view of sections of the event horizon $\mathcal{S}_h$ and the boundary of the ergosphere $\mathcal{S}_s$ for a fixed $a = 0.9$. (a) Sections formed by the intersection with the plane $z = 0$. (b) Sections formed by the intersection with the plane $y = 0$ (gray denotes the region where the ergosphere lies).

$$\mathcal{N}_e^3 = \{(r,\theta,\varphi) | r > r_+, r^2 - 2r + a^2\cos^2\theta < 0\}.$$

As is well known, inside an ergosphere the Boyer-Lindquist coordinates cannot be introduced using material bodies [40]. We show that, nonetheless, their use for parametrization of the timelike geodesics of the Kerr metric (i.e., the trajectories of material particles) will not lead to contradictions everywhere outside the event horizon. To do so, we show that the following inequality always holds for $r > r_+$:

$$\frac{dt}{d\tau} > 0,$$

where τ is the proper time of the particle.

Let us divide both parts of Eq. (1) by $ds^2 = d\tau^2$ and, denoting $u^\alpha = \frac{dx^\alpha}{d\tau}$, consider the function (this function is an analog of the kinetic energy of a particle in classical mechanics)

$$T(\boldsymbol{u}) = \frac{1}{2} g_{\alpha\beta}(r,\theta) u^\alpha u^\beta, \tag{7}$$

the value of which on timelike geodesics is, by definition, equal to $1/2$. It follows from the choice of the signature of the metric that, for each fixed pair of values of r, θ $(r > r_+)$, the three-dimensional surface

$$T(\boldsymbol{u}) = \frac{1}{2} \tag{8}$$

in $\mathbb{R}^4_{\boldsymbol{u}} = \{\boldsymbol{u}\}$ is a two-sheet hyperboloid. Since $g_{t\varphi} \neq 0$, the axis Ot is not one of its principal axes, and, generally speaking, it is not obvious that u^t vanishes nowhere on Eq. (8).

To show this, we find extreme values of the function $F = u^t$ on the hyperboloid (8). Using, for example, the method of undetermined Lagrange multipliers, on one of the parts of the hyperboloid (8) we find

$$\frac{dt}{d\tau} \geq u^t_{\min} = \left.\frac{\sqrt{(r^2+a^2)^2 - a^2\Delta\sin^2\theta}}{\rho\sqrt{\Delta}}\right|_{r>r_+} > 0. \tag{9}$$

Accordingly, on the second half of the hyperboloid (8), $u^t_{\max} = -u^t_{\min}$.

As a consequence, we obtain the well-known fact that in spacetime with a Kerr metric above the event horizon (6) there is no close timelike geodesics.

It follows from the definition of the surface (8) that on one half (the connected component) of the hyperboloid (8) one has $ds = d\tau$, and on the other half $ds = -d\tau$. Therefore, if we adopt the convention that the positive direction of the flow of proper time is toward the future, then the half of the hyperboloid where $ds = -d\tau$ needs to be discarded. Throughout of the rest of this paper we restrict our attention to the part of the surface (8) on which the following relation is satisfied:

$$ds = d\tau.$$

B. Equations of motion of a material point and their integration

We now consider the inertial motion of a material point (particle) in a gravitational field which is described by the Kerr metric outside the event horizon. Its trajectories (world lines) are timelike (i.e., $ds^2 > 0$) geodesic metrics (1) on the manifold $\mathcal{N}^4$. In this section we will use a natural parametrization of these trajectories $\boldsymbol{x}(\tau)$, where τ is the proper time of the particle, the increase of which is directed into the future (i.e., for this choice of units we have $ds = d\tau$.)

1. Hamiltonian representation

It turns out that in this case, both when the equations of motion are explicitly integrated and when a qualitative analysis of the dynamics is carried out, it is more convenient to use a Hamiltonian representation. To do so, we perform a standard Legendre transformation from the four-velocities $u^\alpha = \frac{dx^\alpha}{d\tau}$ to momenta using as the kinetic energy the function $T(\boldsymbol{u})$ defined in Eq. (7). This yields

$$p_\alpha = \frac{\partial T(\boldsymbol{u})}{\partial u^\alpha} = g_{\alpha\beta} u^\alpha,$$

$$H = T|_{\boldsymbol{u}\to\boldsymbol{p}} = \frac{1}{2} g^{\alpha\beta} p_\alpha p_\beta = -\frac{\Delta(r)}{2\rho^2} p_r^2 - \frac{1}{2\rho^2} p_\theta^2 + \frac{((r^2+a^2)p_t + a p_\varphi)^2}{2\Delta(r)\rho^2} - \frac{(a p_t \sin^2\theta + p_\varphi)^2}{2\rho^2\sin^2\theta}. \tag{10}$$

In this case, the equations of motion can be written in the canonical form

$$\frac{d\boldsymbol{x}}{d\tau} = \frac{\partial H}{\partial \boldsymbol{p}}, \qquad \frac{d\boldsymbol{p}}{d\tau} = -\frac{\partial H}{\partial \boldsymbol{x}}. \tag{11}$$

Since, according to Eq. (8), the function T has the fixed value $T = 1/2$, it follows that the physically admissible value of the Hamiltonian (10) for the motion of material points is also fixed:

$$H = \frac{1}{2}. \tag{12}$$

Furthermore, since the transformation (10) is linear in velocities, for each pair of values of $r > r_+$ and θ the equation also defines the two-sheet hyperboloid in the space of momenta $\mathbb{R}^4_{\boldsymbol{p}} = \{\boldsymbol{p}\}$. As noted above (see Sec. II A), when the direction of the proper time is fixed $(ds = d\tau)$, the trajectories of particle motion lie only on one half of this hyperboloid, and the other half must be omitted from consideration (see also Sec. III B).

Remark 4.—To obtain the trajectories of light propagation, one needs to set $H = 0$, but we will not consider that case in this paper.

2. Cyclic variables and Noether's integrals

As can be seen, the Hamiltonian (10) does not explicitly depend on the time of a distant observer t or on the angle φ; i.e., they are cyclic coordinates. Therefore, the values of the corresponding momenta (Noether's integrals) remain unchanged:

$$E = p_t = \text{const}, \qquad L = -p_\varphi = \text{const}.$$

From a physical point of view, E is the energy of the material point and L is the projection of its angular momentum onto the symmetry axis of the metric.

We also recall that the cyclicity of the coordinates t and φ is due to the invariance of the system (10) and (11) under the action of the two-dimensional Abelian translation group $G = \{g_{t_0,\varphi_0} | t_0 \in (-\infty, +\infty), \varphi_0 \bmod 2\pi\}$. Its action in configuration space is given in the following obvious way:

$$g_{t_0,\varphi_0}(t, r, \theta, \varphi) = (t + t_0, r, \theta, \varphi + \varphi_0).$$

In other words, this is the isometry group of the Kerr metric, and the corresponding left-invariant (right-invariant) vector fields of this group define the Killing vectors.

If a particle moves in spacetime with a stationary metric for which $g_{0k} = 0$, $k = 1, 2, 3$ (for example, in Minkowski space or in a Schwarzschild metric), then its energy always turns out to be positive. For the Kerr metric, $g_{t\varphi} \neq 0$; therefore, we analyze the region of possible values of the integrals L and E in more detail.

Specifically, we fix the values of r, $\theta (r > r_+)$ and the value of the integral $L = \text{const}$ and find the extreme values of the function $E = p_t$ from the variables p_t, p_r, and p_θ on the level surface of the function (12). It is easy to show that the extremum is reached for $p_r = 0$ and $p_\theta = 0$ and that the corresponding extreme value $p_t(L, r, \theta)$ is defined as a solution to the equation

$$\frac{1}{\Delta\rho^2}\left[(\Delta\rho^2 + 2r(r^2 + a^2))p_t^2 - 4arLp_t - L^2\left(\frac{\Delta}{\sin^2\theta} - a^2\right)\right] = 1.$$

For example, using the method of undetermined multipliers we obtain

$$\frac{\partial}{\partial p_\alpha}\left(E - \lambda\left(H - \frac{1}{2}\right)\right) = 0, \qquad H - \frac{1}{2} = 0, \qquad \alpha = 0, \ldots, 4.$$

Since H_z is homogeneous and quadratic in p_r and p_θ, it follows that $p_r = 0$ and $p_\theta = 0$.

Of the two roots of this equation only the largest root corresponds to the required half of the surface (12) on which $ds = d\tau$ holds, and it is this root that defines the required minimum of energy E (the smaller root corresponds to the half with $ds = -d\tau$). Accordingly, after some simplifications we obtain a solution of the form

$$\begin{aligned} E_{\min} &= \frac{2arL + \sqrt{D}}{A}, \\ A &= \Delta\rho^2 + 2r(r^2 + a^2) > 0, \\ D &= (2arL)^2 + A\left(L^2\left(\frac{\Delta}{\sin^2\theta} - a^2\right) + \Delta\rho^2\right) \\ &= 4\Delta\rho^2\left(\frac{\rho^2 L^2}{\sin^2\theta} + A\right) > 0. \end{aligned} \tag{13}$$

Now, using this representation for the smallest possible value of energy at the corresponding point of space with the coordinates r and θ with the fixed integral L, we can draw the following conclusions about the region of possible values of L and E (see Fig. 2).

(1) If the point r, θ lies outside the ergosphere (i.e., $\frac{\Delta}{\sin^2\theta} - a^2 > 0$), then, according to Eq. (13),

$$\sqrt{D} > 2ar|L|,$$

and hence the particle's energy E always turns out to be larger than zero (the exact minimum value of E depending on L in this situation will be given below; see Sec. III).

(2) If the values of r, θ correspond to a point inside the ergosphere, then, according to Eq. (13), an exact minimum is reached for $D = 0$, i.e., at the event horizon (with $\Delta = 0$), and hence

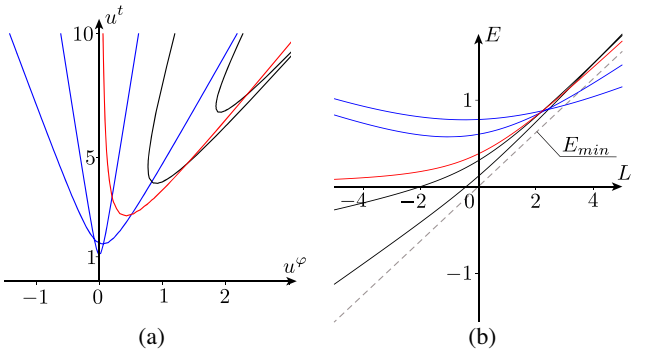

FIG. 2. The boundary of the surface $T = 1/2$ for the fixed $a = 0.9$ and $\theta = \pi/2$ (i.e., for $u^r = 0$ and $u^\theta = 0$) on the plane u^φ, u^t (a) and the boundary of the surface $H = 1/2$ (i.e., when $p_r = 0$ and $p_\theta = 0$) on the plane L, E (b) for different values of r. Black and red lines correspond to the values of r lying in the ergosphere and on its boundary, and blue lines denote the values of r lying beyond the ergosphere.

$$E > E_{\min} = \frac{aL}{r_+^2 + a^2} = \frac{a}{2(1+\sqrt{1-a^2})} L. \qquad (14)$$

As we see, when L are negative, negative values of the particle's energy E are also possible.

Thus, we obtain the following simple result.

Proposition 1.—Suppose that at the initial time $t = 0$ the material point is inside an ergosphere and its energy is negative: $E < 0$. Then it does not leave the ergosphere as $t \to \pm\infty$.

3. Reduction and explicit integration

We make use of the symmetry corresponding to the cyclic variables t and φ and perform a Routh reduction. To obtain a system in a form more typical for mechanics, we make the change of variables

$$p_r \to -p_r, \qquad p_\theta \to -p_\theta, \qquad H \to -\hat{H}.$$

As a result, we obtain a *Hamiltonian natural system with 2 degrees of freedom*,

$$\begin{aligned}
&\frac{dp_r}{d\tau} = -\frac{\partial \hat{H}}{\partial r}, \qquad \frac{dp_\theta}{d\tau} = -\frac{\partial \hat{H}}{\partial \theta},\\
&\frac{dr}{d\tau} = \frac{\partial \hat{H}}{\partial p_r}, \qquad \frac{d\theta}{d\tau} = \frac{\partial \hat{H}}{\partial p_\theta},\\
&\hat{H} = \frac{1}{2\rho^2}\left(\frac{p_r^2}{\Delta} + p_\theta^2\right) + V,\\
&V = \frac{1}{2\Delta\rho^2}\left(-(\Delta\rho^2 + 2r(r^2+a^2))E^2 \right.\\
&\qquad \left. + 4arEL + \left(\frac{\Delta}{\sin^2\theta} - a^2\right)L^2\right). \qquad (15)
\end{aligned}$$

The phase space of this system has the form

$$\mathcal{M}^4 = \{z = (p_r, p_\theta, r, \theta) | r \in (r_+, +\infty), \theta \in (0, \pi)\} \simeq \mathbb{R}^4,$$

and, as noted above, the trajectories of material particles lie on the fixed level set of the Hamiltonian

$$\hat{H} = -\frac{1}{2}.$$

Remark 5.—One can calculate the Gaussian curvature of the metric corresponding to the kinetic energy of system (15):

$$K = -\frac{r(r^2 - 3a^2\cos^2\theta)}{\rho^6}.$$

We see that if $a^2 < 3/4$, the curvature of the configuration space of system (15) is everywhere negative.

In addition to the Hamiltonian $\hat{H}$, the reduced system (15) has the additional Carter integral [14]

$$F(z) = p_\theta^2 + \left(aE\sin\theta - \frac{L}{\sin\theta}\right)^2 - 2a^2\hat{H}(z)\cos^2\theta. \qquad (16)$$

The physical meaning of the Carter integral was discussed in more detail in Ref. [50]. Thus, we obtain the following well-known result: a Hamiltonian system describing the motion of particles in the Kerr metric is integrable using the Liouville-Arnold theorem.

Since both integrals of system (15) turn out to be quadratic, it can, as is well known [51], be integrated by the method of separation of variables. In this case, r and θ are separating variables, and, therefore, to reduce the problem to quadratures, we fix the common level set of the Carter integral and the value of the Hamiltonian as follows:

$$\hat{H}(z) = -\frac{1}{2}, \qquad F(z) = Q + (L - aE)^2, \qquad (17)$$

where Q is a constant. Now we express, taking into account Eq. (17) from Eqs. (12) and (16), the momenta p_r and p_θ and substitute them into the last two equations of motion of system (15). As a result, we obtain equations of motion for r and θ in the following form:

$$\begin{aligned}
&\left(\frac{dr}{d\tau}\right)^2 = \frac{1}{\rho^4}R(r), \qquad \left(\frac{d\theta}{d\tau}\right)^2 = \frac{1}{\rho^4}\Theta(\theta),\\
&R(r) = (E(r^2+a^2) - aL)^2 - (Q + (L-aE)^2 + r^2)\Delta(r),\\
&\Theta(\theta) = Q - \cos^2\theta\left(a^2(1-E^2) + \frac{L^2}{\sin^2\theta}\right). \qquad (18)
\end{aligned}$$

As can be seen, in order to integrate these equations in explicit form, one needs to rescale time as

$$d\tau = \rho^2(r,\theta)du. \qquad (19)$$

We note that the chosen variables are also separated for the problem regarding two Newtonian centers (see Sec. II A).

Thus, for the trajectory of the reduced system the following is satisfied:

(i) the *region of possible motion* on the plane $\mathbb{R}^2 = \{(r,\theta) | r > r_+, \theta \in (0,\pi)\}$ is defined by the relations

$$R(r) \geq 0, \qquad \Theta(\theta) \geq 0,$$

(ii) the simple zeros r_u and θ_u of the functions

$$R(r_u) = 0, \qquad \Theta(\theta_u) = 0$$

define, respectively, the *turning points* of the variables r and θ.

4. Reconstruction of dynamics

From the known solutions $r(\tau)$ and $\theta(\tau)$ the evolution of the other variables is defined, according to Eq. (11), using the quadratures

$$\rho^2\frac{d\varphi}{d\tau}=\frac{a}{\Delta(r)}(E(r^2+a^2)-aL)-aE+\frac{L}{\sin^2\theta},$$
$$\rho^2\frac{dt}{d\tau}=\frac{r^2+a^2}{\Delta(r)}(E(r^2+a^2)-aL)+aL-a^2E\sin^2\theta. \tag{20}$$

Note that in Eqs. (18) and (20) it is necessary to choose the constants of integrals E, L, and Q in such a way that out of the two parts of the surface $\hat{H}=-1/2$ the part where $ds=d\tau$ is chosen. Also note that, as shown above (see Sec. II A), the right-hand side of the second of Eqs. (20) always turns out to be positive.

5. Whittaker's reduction and completeness of the phase flow

In the phase space of system (11) there are trajectories which reach the event horizon $r=r_+$ in a finite proper time τ. As a result, the part of the Liouville-Arnold theorem which describes the integral manifolds of the system and the flow on them cannot be immediately applied to Eq. (11), since this leads to a violation of the condition of completeness of the flows generated by the first integrals H, L, E, and Q of the system [i.e., the possibility of extending the trajectory to an infinite time interval $(-\infty,+\infty)$; see, e.g., Ref. [10]].

It turns out that in this case completeness can be achieved if the trajectories of particles are reparametrized by the time of a distant observer t, and that, by virtue of Eq. (9), such a reparametrization is correct everywhere since $t(\tau)$ is a monotonically increasing function and, as $r\to r_+$, $t\to\pm\infty$. Moreover, after such a time reparametrization, the system is known [52] to be Hamiltonian. Indeed, let us solve the equation for p_t and denote

$$p_t=-\mathcal{E}(p_r,p_\theta,p_\varphi,r,\theta).$$

Then for the remaining variables we obtain the canonical Hamilton equations

$$\frac{dx^k}{dt}=\frac{\partial\mathcal{E}}{\partial p_k},\qquad \frac{dp_k}{dt}=-\frac{\partial\mathcal{E}}{\partial x^k},\quad k=1,2,3.$$

III. BIFURCATION DIAGRAM AND INTEGRAL SUBMANIFOLDS OF THE REDUCED SYSTEM

We now consider the problem of classifying the types of motion of a material particle in a Kerr metric. First we recall some necessary facts from the theory of integrable Hamiltonian systems (for details, see [4,10]).

Since this system has a pair of cyclic coordinates t and φ on which none of the integrals of motion E, L, H, F depend, we proceed in a standard way: we start with a qualitative analysis and a classification of the trajectories of the reduced system (15), and then we examine what the reconstruction of the dynamics (20) yields.

A. Integral submanifolds and their bifurcations

As shown above, the reduced system (15) is an integrable natural Hamiltonian system with 2 degrees of freedom. According to the Liouville-Arnold theorem, its *general position trajectories* are straight lines (under a suitable choice of coordinates) on the two-dimensional integral submanifolds of the system

$$\mathcal{M}^2_{\boldsymbol{I}}=\left\{(p_r,p_\theta,r,\theta)|\hat{H}(z)=-\frac{1}{2},\right.$$
$$\left.F(z)=Q+(L-aE)^2\right\}, \tag{21}$$

where $\boldsymbol{I}=(L,E,Q)$. In the general position case, these submanifolds can turn out to be disconnected and can consist of one or more connected components, each of which can be of one of three types:

$$\text{i. } \mathbb{R}^2,\ \text{a plane;}$$
$$\text{ii. } \mathbb{R}^1\times\mathbb{S}^1,\ \text{a cylinder;}$$
$$\text{iii. } \mathbb{T}^2\simeq\mathbb{S}^1\times\mathbb{S}^1,\ \text{a torus.} \tag{22}$$

Thus, since on each connected component of the submanifold $\mathcal{M}^2_{\boldsymbol{I}}$ all trajectories are the same, it is first necessary to classify various types and bifurcations of integral submanifolds of the reduced system (15). Hence, the space of values of the first integrals of the system

$$\mathbb{R}^3_{\boldsymbol{I}}=\{\boldsymbol{I}=(L,Q,E)\}$$

splits into regions in which all points $\boldsymbol{I}$ correspond to the same type of $\mathcal{M}^2_{\boldsymbol{I}}$. Some of these regions can correspond to manifolds consisting of several connected components, whereas for other regions $\mathcal{M}^2_{\boldsymbol{I}}\simeq\oslash$ (this implies that for these values of the integrals no motion of the system is possible). These regions are separated from each other by *two-dimensional bifurcation surfaces* $\Sigma\subset\mathbb{R}^3_{\boldsymbol{I}}$ (as the above-mentioned values of the integrals pass through these surfaces, the type of $\mathcal{M}^2_{\boldsymbol{I}}$ changes).

We also note that in this case a *one-dimensional bifurcation curve* $\sigma^\theta\subset\mathbb{R}^3_{\boldsymbol{I}}$ arises in the space of integrals. Its origin is due to the fact that the symmetry group of the system which defines the rotation about the axis Oz has in the phase

space orbits of two types: a one-dimensional orbit—the circle $\mathbb{S}^1$ and a zero-dimensional orbit—points on the symmetry axis P^0. As is well known, a set consisting of orbits of the same type (in this case $\mathcal{M}^0 = \cup P^0$ and $\mathcal{M}^1 = \cup \mathbb{S}^1$) is invariant under the phase flow of the system. Accordingly, for system (10) and (11) motions along the symmetry axis lie on the manifold $\mathcal{M}_0$, and these motions correspond to the values of the integrals that lie on the curve σ^θ.

In the case of a system with separating variables, analysis of the bifurcations of the integral submanifolds $\mathcal{M}^2_{\boldsymbol{I}}$ usually simplifies considerably [4,10]. Indeed, let us write Eqs. (15) in the initial variables $z = (p_r, p_\theta, r, \theta)$ We see that the integral submanifold (21) is represented as the product of a pair of plane curves:

$$\begin{aligned} &\mathcal{M}^2_{\boldsymbol{I}} = \mathcal{C}^1_r \times \mathcal{C}^1_\theta, \\ &\mathcal{C}^1_r = \{(p_r, r) | p_r^2 = \Delta^2(r) R(r), r > r_+\}, \\ &\mathcal{C}^1_\theta = \{(p_\theta, \theta) | p_\theta^2 = \Theta(\theta), 0 < \theta < \pi\}, \end{aligned} \tag{23}$$

which depend on four parameters: a, L, E, and Q. Consequently, the problem regarding restructuring $\mathcal{M}^2_{\boldsymbol{I}}$ reduces to separately investigating the bifurcations of each of the curves, $\mathcal{C}^1_r$ and $\mathcal{C}^1_\theta$.

It follows from Eq. (23) that the structure of $\mathcal{M}^2_{\boldsymbol{I}}$ changes, first, at those values of the integrals $\boldsymbol{I}$ for which the functions $R(r)$ and $\Theta(\theta)$ have zeros which are critical points, i.e.,

$$R(r_c) = 0, \left.\frac{dR}{dr}\right|_{r=r_c} = 0, \quad r_c > r_+, \tag{24}$$

or

$$\Theta(\theta_c) = 0, \left.\frac{d\Theta}{d\theta}\right|_{\theta=\theta_c} = 0, \quad 0 < \theta < \pi. \tag{25}$$

Such bifurcations are called *local*. Second, bifurcations of curves where the behavior of the functions $R(r)$ and $\Theta(\theta)$ changes on the boundaries of their domains of definition are also possible; such bifurcations are called *nonlocal*.

Thus, we finally conclude that for this system, depending on the values of the first integrals $\boldsymbol{I} = L, E, Q$, the following cases are possible.

(1) Let $\boldsymbol{I}$ be such that neither the relation (24) nor the relation (25) is satisfied. Then $\mathcal{M}^2_{\boldsymbol{I}}$ is a set of two-dimensional submanifolds from the list in Eq. (22).

(2) If $\boldsymbol{I}$ is such that only one of the relations (24) and (25) is satisfied, then, first, one or several (one-dimensional) curves corresponding to the partial solutions of the system (15), called *critical solutions* [4,10], enter $\mathcal{M}^2_{\boldsymbol{I}}$. Second, if any of these solutions are orbitally unstable [i.e., a critical point in Eq. (24) or (25) is a minimum], then two-dimensional surfaces formed by the trajectories asymptotically approaching the corresponding unstable orbit as $\tau \to \pm\infty$ also enter $\mathcal{M}^2_{\boldsymbol{I}}$.

(3) If $\boldsymbol{I}$ is such that both systems (24) and (25) simultaneously have a solution, then $\mathcal{M}^2_{\boldsymbol{I}}$ is formed by the fixed points of system (15), and, if any of these points are unstable, the submanifolds adjacent to these (unstable) points and filled with asymptotic curves also enter $\mathcal{M}^2_{\boldsymbol{I}}$.

B. Elimination of nonphysical components

It is important to keep in mind that in investigating the reduced system (15) we eliminate from consideration the evolution of the time of the distant observer $t(\tau)$, which, according to Eq. (9), is given by a *monotonically increasing function*. As a result, for some components of the integral surface $\mathcal{M}^2_{\boldsymbol{I}}$ of the reduced system (15), it turns out that $\frac{dt}{d\tau} < 0$, so they need to be eliminated.

Indeed, the equations of motion of the reduced system (11) are quadratic and homogeneous in the variables L and E and hence are invariant under the change of variables

$$L \to -L, \qquad E \to -E, \qquad Q \to Q, \tag{26}$$

i.e., under rotation through 180° about the axis OQ in the space $\mathbb{R}^3_{\boldsymbol{I}}$. At the same time, under this transformation the right-hand sides change sign in Eqs. (20), which govern the evolution of φ and t.

To ascertain what exactly needs to be eliminated, we represent Eq. (20) for t as

$$\frac{dt}{d\tau} = E + \frac{2r(r^2 + a^2)}{\rho^2 \Delta}\left[E - \frac{aL}{r^2 + a^2}\right]. \tag{27}$$

We also note that, according to Eq. (9), the function $\frac{dt}{d\tau}$ has the same sign on the entire connected component of the integral submanifold $\mathcal{M}^2_{\boldsymbol{I}}$, so it suffices for us to examine only the limiting cases of this ratio for $r \to +\infty$ and $r \to r_+$.

We first set $r = r_+ + \varepsilon$, $0 < \varepsilon \ll 1$ in relation (27):

$$\frac{dt}{d\tau} = \frac{1}{\varepsilon}\frac{r_+(r_+^2 + a^2)}{\sqrt{1 - a^2}}\left(E - \frac{aL}{r_+^2 + a^2}\right) + O(1).$$

This implies that, if

$$E < \frac{aL}{r_+^2 + a^2}, \tag{28}$$

then on the part of the curve $\mathcal{C}^1_r$ which is adjacent to the event horizon (and to the corresponding component of the integral submanifold $\mathcal{M}^2_{\boldsymbol{I}}$) the following inequality holds:

$$\frac{dt}{d\tau} < 0.$$

That is, this component must be excluded as a nonphysical one. In other words, under condition (28) there are no trajectories that approach the horizon.

In a similar way, it is proved that if

$$E < 0,$$

then there are no physical (i.e., such that $\frac{dt}{d\tau} > 0$) components $\mathcal{M}^2_{\boldsymbol{I}}$ for which $r \to +\infty$. Indeed, according to Eq. (27), as $r \gg 1$,

$$\frac{dt}{d\tau} = E + O\left(\frac{1}{r}\right) < 0 \quad \text{for } E < 0.$$

For bounded components of $\mathcal{M}^2_{\boldsymbol{I}}$ which are not adjacent to the event horizon, the reasoning presented here turns out to be inapplicable. However, owing to invariance of the reduced system under the change of variables (26), the pairs of its invariant submanifolds that are related by this transformation turn out to be equivalent to

$$\mathcal{M}^2_{L,E,Q} \simeq \mathcal{M}^2_{-L,-E,Q}.$$

On the other hand, relation (27) changes sign under such a transformation. This implies that one of the components of these submanifolds must be eliminated as a nonphysical one. By straightforward verification it can be shown that bounded components of $\mathcal{M}^2_{\boldsymbol{I}}$ which are not adjacent to the horizon $r = r_+$ are physical if for them $E > 0$.

Remark 6.—As shown in Sec. II A [see (9)] the sign of $\frac{dt}{d\tau}$ cannot change under any deformations of the surface $\mathcal{M}^2_{\boldsymbol{I}}$ under which it does not touch the event horizon. Consequently, it suffices to calculate $\frac{dt}{d\tau}$ for the bounded component of the curve $\mathcal{C}^1_r$ for some fixed values $\boldsymbol{I}_0 = (L_0, E_0, Q_0)$ since throughout the region bounded by the bifurcation surfaces the sign of $\frac{dt}{d\tau}$ for this region remains unchanged.

C. Analysis of the curves $\mathcal{C}^1_\theta$

We first note that the equation for $\mathcal{C}^1_\theta$ can be represented as

$$p^2_\theta + U_\theta = Q = \text{const},$$
$$U_\theta = Q - \Theta(\theta) = \cos^2\theta\left[a^2(1-E^2) + \frac{L^2}{\sin^2\theta}\right].$$

Since U_θ does not depend on Q, the analysis of the curves $\mathcal{C}^1_\theta$ is entirely similar to the analysis of trajectories in the phase space $\mathbb{R}^2 = \{(\theta, p_\theta)\}$ for the Hamiltonian system describing the motion of a material point in a potential field U_θ (the function U_θ is sometimes called a *latitudinal potential* [21]), and the constant Q is similar to the level set of the energy integral. As is well known, ascertaining the type of these trajectories reduces to analyzing the behavior of the function U_θ on the interval $\theta \in (0, \pi)$.

First, we note that the function U_θ is symmetric about the straight line $\theta = \pi/2$, i.e.,

$$U_\theta\left(\frac{\pi}{2} + x\right) = U_\theta\left(\frac{\pi}{2} - x\right).$$

Second, if $\theta = \pi/2$, this function vanishes and simultaneously has a critical point:

$$U_\theta\left(\frac{\pi}{2}\right) = 0, \qquad \left.\frac{dU_\theta}{d\theta}\right|_{\theta=\pi/2} = 0.$$

Third, the numerator of the function is a fourth-order polynomial in the variable $u = \cos\theta$. Therefore, in addition to the (multiple) roots, the function $U_\theta(u)$ can have a pair of roots when $\theta = \pi/2$ ($u = 0$).

Moreover, if $L \neq 0$, the function increases without bounds as $\theta \to 0$ and $\theta \to \pi$, while if $L = 0$, on the boundaries this function takes the finite values $U_\theta(0) = U_\theta(\pi) = a^2(1-E^2)$.

Let us define the constant value

$$C_1 = a^2(E^2 - 1) - L^2,$$

which is proportional to the second derivative of the function U_θ in $\theta = \pi/2$. Depending on the sign of C_1 and the value of L, four qualitatively different types of the function U_θ are possible, each of which corresponds to the family of curves (25), which are parametrized by the value of the integral Q (see Figs. 3 and 4).

We now construct the corresponding bifurcation surfaces $\Sigma^\theta \subset \mathbb{R}^3_{\boldsymbol{I}}$ by making use of Eqs. (25). The critical point in $\theta = \pi/2$ corresponds to the plane in the space of the integrals

$$\Sigma^\theta_0 = \{(L, Q, E) | Q = 0\}.$$

The minimum of the function U_θ with $Q < 0$ [see Fig. 3(b)] corresponds to the surface consisting of two parts,

$$\Sigma^\theta_{\min} = \Sigma^\theta_+ \cup \Sigma^\theta_-,$$
$$\Sigma^\theta_+ = \left\{(L, E, Q) | L > 0, Q < 0, \right.$$
$$\left. E^2 - \frac{1}{a^2}(L + \sqrt{-Q})^2 = 1\right\},$$
$$\Sigma^\theta_- = \left\{(L, E, Q) | L < 0, Q < 0, \right.$$
$$\left. E^2 - \frac{1}{a^2}(L - \sqrt{-Q})^2 = 1\right\}.$$

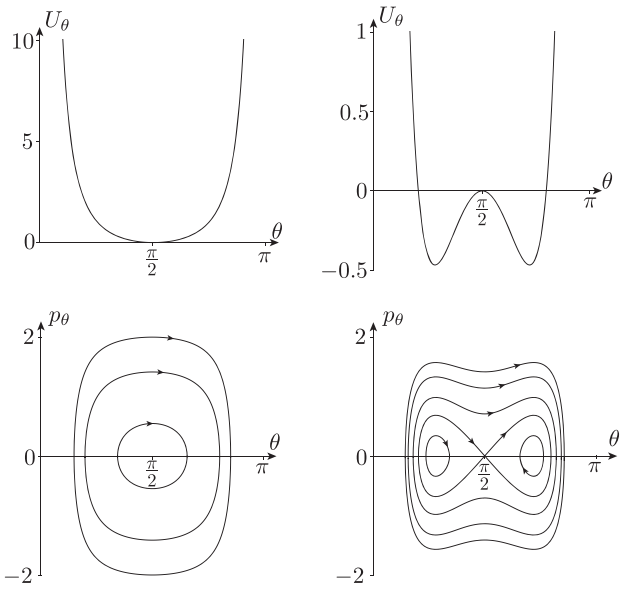

(a) $C_1 < 0$ $(E = 0.5)$ (b) $C_1 > 0$ $(E = 5.7)$

FIG. 3. Typical view of the latitudinal potential U_θ and the corresponding curves $\mathcal{C}^1_\theta$ on the plane $(\theta,\ p_\theta)$ with $L \neq 0$ and different values of C_1 for a fixed $a = 0.3$ and $L = 1$.

As can be seen, two parts of this surface are symmetric about the plane $L = 0$, i.e., $\Sigma^\theta_+ \to \Sigma^\theta_-$ as $L \to -L$, and at each fixed value of $Q \leq 0$ they are parts of a hyperbola. When $Q = 0$, the surfaces Σ^θ_+ and Σ^θ_- form one smooth curve for which $C_1 = 0$.

The extremum of the function U_θ with $L = 0$ [see Fig. 4(b)] corresponds to the bifurcation curve (mentioned above)

$$\sigma^\theta = \{(L, E, Q) | L = 0, Q = a^2(1 - E^2)\}.$$

We now sum up the results described above and relating to the analysis of the form of the curve $\mathcal{C}^1_\theta$ depending on the values of the integrals. We assume that the axis OQ in the space $\mathbb{R}^3_I$ is vertical. Accordingly, the upward direction corresponds to an increase in the values of Q, while the downward direction corresponds to a decrease in Q; see Fig. 5.

(1) If $C_1 < 0$, then the region of possible values of the integrals in $\mathbb{R}^3_I$ is bounded from below by the plane Σ^θ_0; in this case the motion of a particle in the equatorial plane $\theta = \pi/2$ is stable.

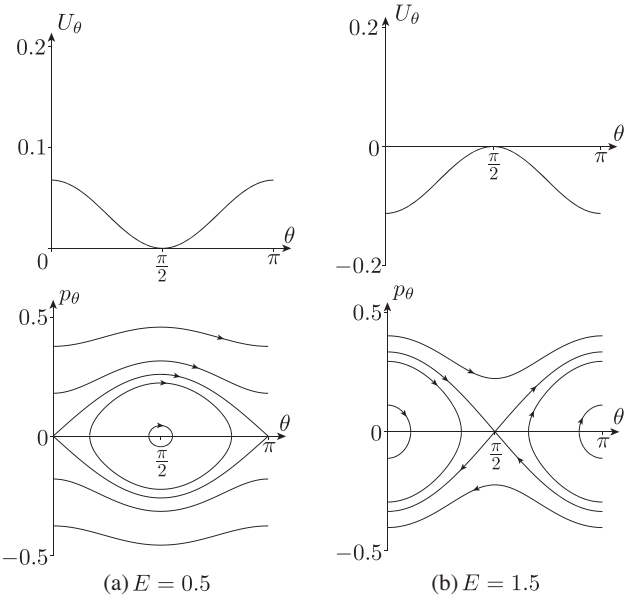

(a) $E = 0.5$ (b) $E = 1.5$

FIG. 4. Typical view of the latitudinal potential U_θ and the corresponding curves $\mathcal{C}^1_\theta$ on the plane $(\theta,\ p_\theta)$ with different values of C_1 for a fixed $a = 0.3$ and $L = 0$.

(2) If $C_1 > 0$, then the region of possible values of the integrals in $\mathbb{R}^3_I$ is bounded from below by the surface $\Sigma^\theta_{\min}$; in this case the motion of a particle in the equatorial plane $\theta = \pi/2$ is unstable.

(3) If $Q > 0$, then, as the graph U_θ in Fig. 3 implies, for any $L \neq 0$ the curve $\mathcal{C}^1_\theta \simeq \mathbb{S}^1$ is a connected curve and intersects with the equatorial plane.

(4) If $Q < 0$ and $C_1 > 0$ (i.e., the point $\boldsymbol{I}$ corresponding to the values of the integrals lies between the surfaces $\Sigma^\theta_{\min}$ and Σ^θ_0), then, as the graph U_θ in Fig. 3(b) implies, for any $L \neq 0$ the curve $\mathcal{C}_\theta \simeq \mathbb{S}^1 \cup \mathbb{S}^1$

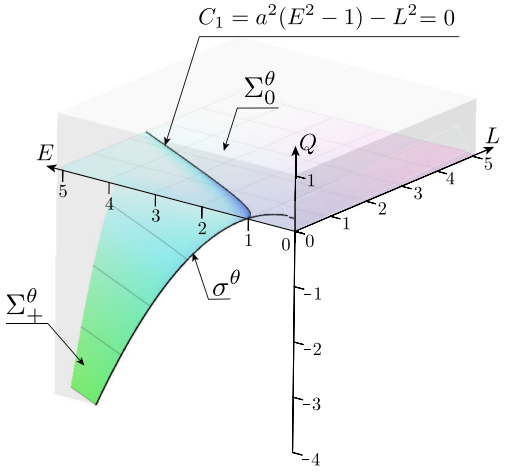

FIG. 5. Structure of bifurcation surfaces and curves in the space of first integrals $\mathbb{R}^3_I$ for a fixed $a = 0.5$. Gray denotes the region of possible values of L, E, and Q.

consists of two closed curves which do not intersect with the equatorial plane.

D. Analysis of the curves $\mathcal{C}_r^1$

Since the function $\Delta(r)$ is always positive on the interval $r \in (r_+, +\infty)$, the analysis of the curve $\mathcal{C}_r^1$ reduces in fact to investigating the behavior of the zeros of the function

$$\begin{aligned} R(r) &= (E(r^2+a^2) - aL)^2 \\ &\quad - (Q + (L-aE)^2 + r^2)\Delta(r) \\ &= (E^2-1)r^4 + 2r^3 + (a^2(E^2-1) - L^2 - Q)r^2 \\ &\quad + 2(Q + (L-aE)^2)r - a^2 Q, \end{aligned} \tag{29}$$

depending on the parameters a, Q, E, and L.

This function is a fourth-degree polynomial and therefore has no more than 4 roots. We also note that

$$R(r_+) \geq 0, \tag{30}$$

and that the zero value is only reached at the boundary of the region of possible values of L and E inside the ergosphere.

It follows from Eqs. (29) and (30) that, if $E^2 - 1 < 0$, then $R(r) \to_{r\to+\infty} -\infty$. Therefore, on the interval $r \in (r_+, +\infty)$ the polynomial $R(r)$ can have only an odd number of roots, i.e., 1 or 3. Accordingly, if $E^2 - 1 > 0$, then $R(r) \to_{r\to+\infty} +\infty$, and if $r > r_+$, there can in principle be 0, 2, or 4 roots. However, according to Descartes's rule of signs, if all roots of a polynomial are positive, then no neighboring coefficients in its power expansion can have the same sign. Consequently, the polynomial (29) with $E^2 - 1 > 0$ cannot have 4 roots on the interval $(r_+, +\infty)$ since the signs at the coefficients r^3 and r^4 coincide.

Thus, we finally find that on the interval $r \in (r_+, +\infty)$ the function $R(r)$ can have

(a) if $E^2 < 1$, either 1 or 3 roots (see Fig. 6),
(b) if $E^2 > 1$, either 0 or 2 roots (see Fig. 7).

We now construct the corresponding bifurcation surfaces $\Sigma^r \subset \mathbb{R}^3_I$.

1. Nonlocal bifurcations

These bifurcations are not described by Eqs. (24), and the bifurcations of the curve C_r^1 are due to changes in the behavior of the function $R(r)$ on the boundaries of the interval $(r_+, +\infty)$.

First, we see that, according to Eq. (29), if the expression $(E^2 - 1)$ changes sign, the behavior of $R(r)$ changes as $r \to +\infty$. It should be kept in mind that outside the ergosphere (in particular, as $r \to +\infty$) the energy $E > 0$ (see Sec. II B); therefore, the value $E = -1$ must be eliminated (for details, see Sec. III B). Thus, the corresponding surface in $\mathbb{R}^3_I$ which defines such a nonlocal bifurcation has the form

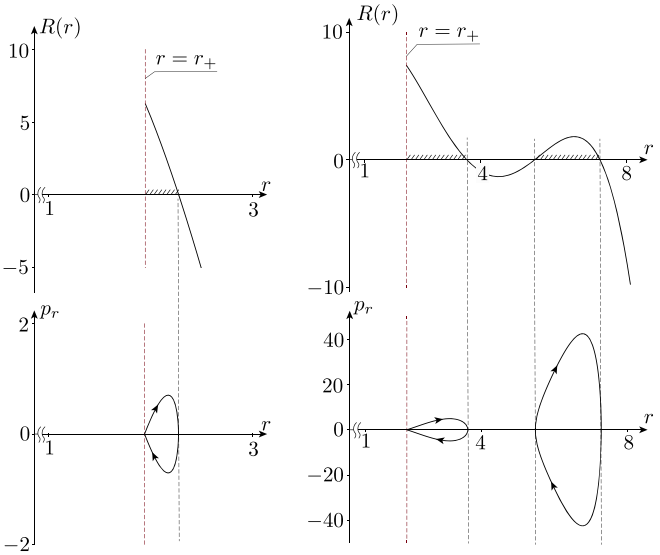

(a) $L = 4, E = 0.95, Q = 1$ (b) $L = 3.2, E = 0.937, Q = 0.9$

FIG. 6. The function $R(r)$ and the corresponding curves $\mathcal{C}_r^1$ on the plane (r, p_r) for a fixed $a = 0.3$ with $E < 1$.

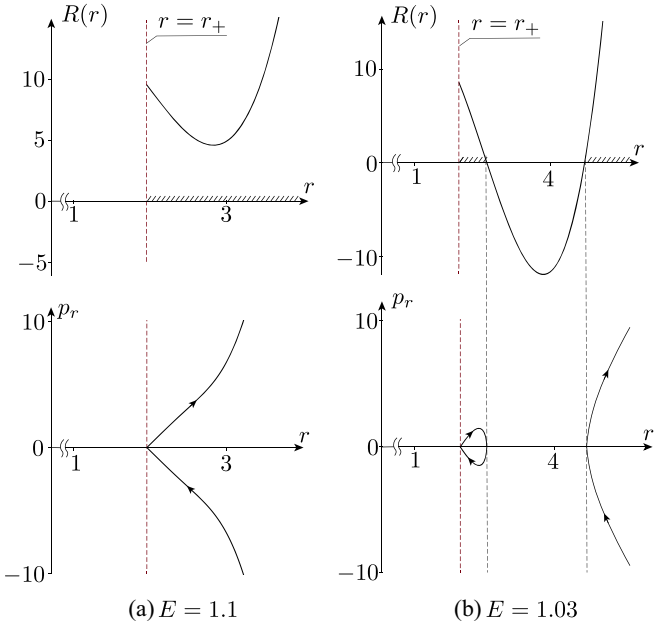

(a) $E = 1.1$ (b) $E = 1.03$

FIG. 7. The function $R(r)$ and the corresponding curves $\mathcal{C}_r^1$ on the plane (r, p_r) for a fixed $a = 0.3$, $L = 4$, $Q = 1$, with $E > 1$.

$$\Sigma^r_\infty = \{(L, E, Q) | E = 1\}.$$

The energy $E = 1$ has the meaning of the *escape energy* of a particle from the black hole. In the Kepler problem, the escape velocity is treated in a similar way.

It is also important to keep in mind that, when $Q < 0$, the bifurcation surface Σ^r_∞ lies outside the region of possible values of the integrals L, E, and Q, which is bounded by the surface $\Sigma^\theta_{\min}$ (see Sec. III C).

Second, we note that Eq. (29) also implies that $R(r_+) \geq 0$, and also that, if

$$E = \frac{a}{a^2 + r_+^2} L = \frac{a}{2(1 + \sqrt{1 - a^2})} L, \tag{31}$$

the region of positive values of $R(r)$ adjacent to the horizon $r = r_+$ disappears (shrinks to a point). We also recall that, according to the results in Sec. II B, the condition $\frac{dt}{d\tau} > 0$ is not satisfied for the values of the integrals L and E lying under the straight line (31) (see Sec. III B for details), and therefore no motion is possible. Thus, we find another surface of nonlocal bifurcations of the following form:

$$\Sigma^t = \{(L, E, Q) | E(r_+^2 + a^2) - aL = 0\}.$$

When the path in the space of values of the integrals crosses this surface, the regions of possible particle motions in a neighborhood of the event horizon appear or disappear (depending on the direction of the intersection).

2. Local bifurcations

We now turn to analysis of bifurcation surfaces given by relations (24). Since in this case it is impossible to explicitly solve these equations for r_c, we will represent the required surfaces in the parametric form $E(r_c, Q)$, $L(r_c, Q)$.

Since this transformation maps the solution to Eqs. (24) into other solutions, we first restrict our attention to these bifurcation surfaces under the condition

$$E \geq 0$$

because the surfaces with $E < 0$ can finally be constructed by the rotation (26).

The following proposition holds.

Proposition 2.—Let L, E, and Q be possible values of the integrals bounded by the surfaces Σ_0^θ, $\Sigma_{\min}^\theta$ (see Sec. III C). Then the local bifurcations of the curves C_r^1 are possible only for

$$Q \geq 0.$$

We note that, according to the analysis in Sec. III C, the possible values of integrals L and E satisfy the following inequality for $Q < 0$:

$$a^2(E^2 - 1) - L^2 \geq 0. \tag{32}$$

Eliminating from Eqs. (24) the terms containing the product EL, we obtain an equation satisfied by the critical values of E, L, and Q in the form

$$r_c^2 L^2 - r_c^2(3r_c^2 + a^2)(E^2 - 1) + Q(r_c^2 - a^2) - 4r_c^2 = 0.$$

Expressing L from this relation and substituting it into Eq. (32), we obtain the inequality

$$-3r_c^2(E^2 - 1) - \frac{r_c^2 + a^2}{r_c^2}(-Q) - 4r_c \geq 0,$$

which cannot be satisfied for

$$a < r_+ < r_c, \qquad Q < 0.$$

Hence, under condition (32) (i.e., when $Q < 0$) system (24) has no solution.

System (24), which defines the critical points $r = r_c$, is a system of two homogeneous quadratic equations in L and E. As is well known, this system can be reduced to a homogeneous biquadratic equation. In this case we obtain an equation of the form

$$\begin{aligned} G(X) &= AX^2 - 2BX + C = 0, \\ A &= r_c^4(r_c(r_c - 3)^2 - 4a^2), \qquad C = r_c C_0^2, \\ C_0 &= r_c(r_c - 2)^2 - a^2\left(1 + \frac{r_c - 1}{r_c^2} Q\right), \\ B &= r_c^4(r_c - 3)(r_c - 2)^2 - r_c^3(3r_c - 5)a^2 \\ &\quad - r_c(r_c^2 - 4r_c + 5)a^2 Q + 2a^4 Q. \end{aligned} \tag{33}$$

The correspondences between its solutions and the solutions of system (24) are as follows:

$$\begin{aligned} X_+(r_c, Q) &= \frac{B + \sqrt{B^2 - AC}}{A}, \qquad E_+(r_c, Q) = \sqrt{X_+}, \\ L_+(r_c, Q) &= \frac{1}{2a\sqrt{X_+}}(C_0 - (r_c^2(r_c - 3) - 2a^2)X_+), \end{aligned} \tag{34a}$$

$$\begin{aligned} X_-(r_c, Q) &= \frac{B - \sqrt{B^2 - AC}}{A}, \qquad E_-(r_c, Q) = \sqrt{X_-}, \\ L_-(r_c, Q) &= \frac{1}{2a\sqrt{X_-}}(C_0 - (r_c^2(r_c - 3) - 2a^2)X_-). \end{aligned} \tag{34b}$$

This yields a surface in the space of first integrals $\mathbb{R}_I^3$ which consists of two parts,

$$\begin{aligned} \Sigma_0^r &= \Sigma_+^r \cup \Sigma_-^r, \\ \Sigma_+^r &= \{(L, E, Q) | E = E_+(r_c, Q), L = L_+(r_c, Q), Q \geq 0\}, \\ \Sigma_-^r &= \{(L, E, Q) | E = E_-(r_c, Q), L = L_-(r_c, Q), Q \geq 0\}. \end{aligned}$$

Remark 7.—If $Q = 0$, then after simplifications the equations for Σ_0^r can be represented as

$$E_\pm = \frac{r_c^{3/2} - 2r_c^{1/2} \pm a}{r_c^{3/4}(r_c^{3/2} - 3r_c^{1/2} \pm 2a)^{1/2}},$$
$$L_\pm = \pm\frac{r_c^2 \mp 2ar_c^{1/2} + a^2}{r_c^{3/4}(r_c^{3/2} - 3r_c^{1/2} \pm 2a)^{1/2}}, \qquad (35)$$

where the upper sign refers to E_+ and L_+, and the lower sign to E_- and L_-.

Equation (33) has a number of remarkable features which allow a fairly complete analysis of the behavior of its solutions depending on the parameters, and hence enable an analysis of the surface Σ_0^r.

First, we see that, when $r_c > r_+$,

$$C(r_c, Q) \geq 0.$$

Thus, from Eq. (34) we draw the following conclusions.

(i) If $A < 0$, then Eq. (33) always has two real roots, one of which is negative (i.e., must be discarded):

$$X_+(r_c, Q) < 0, \qquad X_-(r_c, Q) > 0.$$

(ii) If $A > 0$ and $B > 0$, then Eq. (33) either has no real roots or both of them are positive:

$$X_+(r_c, Q) > 0, \qquad X_-(r_c, Q) > 0.$$

(iii) If $A > 0$ and $B < 0$, then Eq. (33) either has no roots or both of them are negative (i.e., they must be discarded):

$$X_+(r_c, Q) < 0, \qquad X_-(r_c, Q) < 0.$$

Second, the coefficient A does not depend on Q, and all its roots are found explicitly by the trigonometric parametrization:

$$A(r_c) = r_c^4 \prod_{k=0}^{2}(r - r_k(\alpha)), \qquad r_k = 4\sin^2\left(\alpha + \frac{2\pi}{3}k\right),$$
$$a(\alpha) = \sin 3\alpha, \qquad 0 \leq \alpha \leq \pi/6,$$

and for any value of a the roots r_k satisfy the following inequalities (see Fig. 8):

$$0 \leq r_0 \leq 1 \leq r_+ \leq r_1 < 3 \leq r_2 \leq 4.$$

Consequently, the surface $r = r_2(a) = \text{const}$ corresponding to the largest root lies, at all values of a, outside the ergosphere, whereas part of the surface $r = r_1(a) = \text{const}$ with $(a > a_* = \frac{1}{\sqrt{2}}$, i.e., $\alpha > \frac{\pi}{12})$, which is near the equator $\theta = \pi/2$, turns out to lie inside the ergosphere.

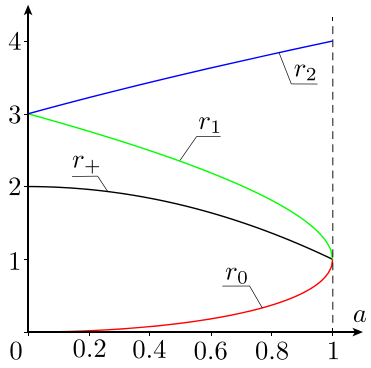

FIG. 8. Dependence of the roots of the equation $A(r_c) = 0$ on the parameter a.

Third, both for large r_c and for $a = 0$, Eq. (33) simplifies to

$$G(X)|_{a=0} = r_c^7\left(X - \frac{(r_c - 2)^2}{r_c(r_c - 3)}\right)^2 = 0.$$

It follows that for $X_\pm \underset{r_c\to+\infty}{\longrightarrow} 1$ and according to Eq. (34), we obtain

$$E_+ \underset{r_c\to+\infty}{\longrightarrow} 1 - 0, \qquad L_+ \underset{r_c\to+\infty}{\longrightarrow} -\infty,$$
$$E_- \underset{r_c\to+\infty}{\longrightarrow} 1 - 0, \qquad L_- \underset{r_c\to+\infty}{\longrightarrow} \infty.$$

This implies that, on the plane of values of the coefficients (A, B) with any fixed a and $Q \geq 0$, the curve $\Gamma_{AB}(r_c) : (A(r_c), B(r_c))$ with large r_c lies in the first quadrant (i.e., $A > 0$, $B > 0$). On the other hand, $A(r_+) > 0$, and for $Q \geq 0$ we have

$$B = \Delta(r_c)[r_c^3(r_c^2 - 5r_c + 6) + (r_c - 2)a^2Q] - r_c^3(r_c - 1)^2a^2 - r_c(1 - a^2)a^2Q|_{r_c=r_+} \leq 0.$$

Therefore, the curve $\Gamma_{AB}(r_c)$ starts at $r_c = r_+$ in the second quadrant and intersects with the axis $A = 0$ twice as $r_c \to \infty$ since $A(r_c)$ has two roots on the interval $(r_+, +\infty)$. Consequently, three general position cases for the structure of the curve Γ_{AB} are in principle possible (see Fig. 9).

Remark 8.—In this case, in order to give a rigorous proof in which only the situations shown in Fig. 9 are possible, it is also necessary to show that, when $0 < a \leq 1$ and $Q \geq 0$, the coefficient $B(r_c)$ has only one root on the interval $(r_+, +\infty)$. The rigorous proof known to us is based on Sturm's theorem and is so cumbersome that we do not present it here.

We show that the situation in Fig. 9(c) does not take place for $a^2 > 0$ and $Q \geq 0$. To do so, we calculate $B(r_k)$ using the above-mentioned parametrization of the roots $A(r)$:

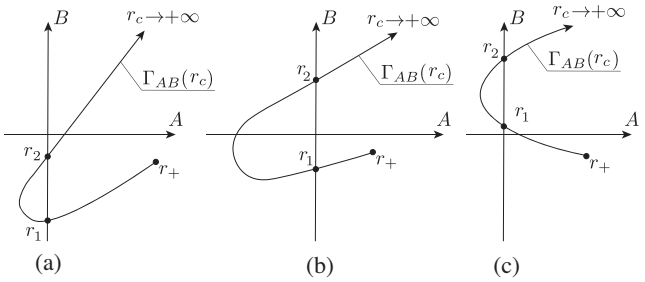

FIG. 9. Possible positions of the curve Γ_{AB}.

$$B(r_k) = -2a\sin^2\alpha_k(1-4\sin^2\alpha_k)^2(32\sin^5\alpha_k + aQ),$$
$$a = \sin 3\alpha, \quad \alpha_k = \alpha + \frac{2\pi}{3}k, \quad k = 0,1,2, \quad \alpha \in \left(0, \frac{\pi}{6}\right).$$

This implies that

$$B(r_1) < 0 \quad \text{for } Q \geq 0,$$
$$B(r_2) < 0 \quad \text{for } Q > Q_c^{(1)}, \qquad Q_c^{(1)} = \frac{32\sin(\alpha+\pi/3)}{\sin 3\alpha},$$
$$B(r_2) > 0 \quad \text{for } 0 \leq Q < Q_c^{(1)}.$$

Thus, the segment of the curve $\Gamma_{AB}(r_c)$ with $r_c \in (r_+, r_1)$ always enters region iii.

Fourth, the discriminant of Eq. (33) is factored in such a way that

$$\hat{D}(r_c, Q) = B^2 - AC = 4a^2\Delta^2(r_c)P_Q(r_c),$$
$$P_Q(r_c) = r_c^5 - r_c^3(r_c - 3)Q + a^2Q^2.$$

Accordingly, for sufficiently small positive Q for all $r_c > r_+$ it turns out that $P_Q(r_c) > 0$. In addition, for all $a \in [0, 1]$ the relation $r_+(a) \leq 2$ is satisfied, and hence for $Q > 0$ we obtain

$$P_Q(r_+) = r_+^5 + r_+^3(3 - r_+)Q + a^2Q^2 > 0.$$

Consequently, for each fixed a, the critical values of $Q_c(a)$ at which the polynomial $P_Q(r_c)$ has roots on the interval $(r_+, +\infty)$ are defined by the following conditions:

$$P_Q(r_c) = 0, \frac{dP_Q(r_c)}{dr_c} = 0, \qquad r_c > r_+.$$

These equations lend themselves to a fairly simple analysis since the second of them reduces to the following quadratic equation in r_c:

$$\frac{dP_Q}{dr_c} = r_c^2(5r_c^2 - 4Qr_c + 9Q). \tag{36}$$

It has nonzero real solutions (for positive Q) only under the condition $Q \geq 45/4$. We make use of the following parametrization:

$$Q = \frac{45}{4 - x^2}, \qquad x \in [0, 2).$$

Then the nonzero roots $r_c^{(+)}$ and $r_c^{(-)}$ of Eq. (36) can be represented as

$$\frac{9}{4} < r_c^{(-)} = \frac{9}{2+x} < \frac{9}{2} < r_c^{(+)} = \frac{9}{2-x}.$$

Substituting into these values from Eq. (36), we find

$$P_2(r_c^{(-)}) = \frac{3^9}{(4-x^2)^2}\left(\frac{25}{243}a^2 + \frac{(2-x)(2x+1)}{(2+x)^3}\right),$$
$$P_2(r_c^{(+)}) = \frac{3^9}{(4-x^2)^2}\left(\frac{25}{243}a^2 + \frac{(2-x)(1-2x)}{|2+x|^3}\right).$$

We see that, for $a^2 \leq 1$ and $x \in [0, 2)$, the first function is larger than zero everywhere and the second has the only root $x(a)$ near the value $x(0) = 1/2$, which corresponds to the critical values of $Q_c(a)$ which satisfy the relations

$$Q_c(0) \leq Q_c(a) \leq Q_c(1),$$
$$Q_c(0) = 12, \qquad Q_c(1) = \frac{3125}{256} \approx 12.21.$$

Note that this dependence admits a good approximation using the Taylor series:

$$Q_c(a) = 12 + \frac{27}{25}\mu - \frac{4131}{10000}\mu^2 + O(\mu^3), \qquad \mu = \frac{50}{243}a^2.$$

A typical view of the surface Σ_0^r is shown in Fig. 10.

3. Stability of critical solutions

To analyze the stability of the trajectories $r = r_c = \text{const}$, we first consider the case $Q < Q_c$. Figure 10 clearly shows a singularity of the *cusp* type on each of the curves defined by relations (34). A natural question arises: do these curves really contain a singularity or is this because of inaccuracies in constructing the curve, in which case a more detailed enlargement will reveal that the curves are smooth?

To answer this question, we first note that, if $Q = \text{const}$, on each of these curves as $E \to 1$ ($L \to \pm\infty$) the function $R(r)$ has a maximum at the critical point $r = r_c$, whereas at the other end of these curves as $E \to +\infty$ the function $R(r)$ has a minimum. Consequently, in the expansion in a neighborhood of the critical point satisfying Eqs. (24),

$$R(r) = W(L, E)(r - r_c(L, E)) + O(|r - r_c(L, E)|^2)$$

the coefficient $W(L, E)$ changes sign as the parameters change along the bifurcation curves under study. Hence, there is a point of the curve (L_*, E_*) at which

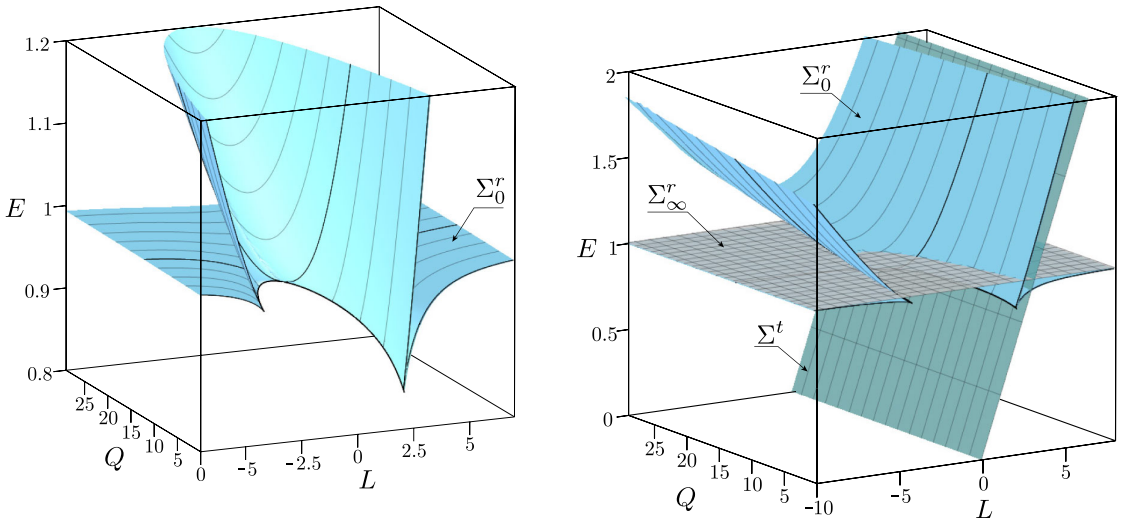

FIG. 10. Arrangement of bifurcation surfaces and curves in the space of first integrals $\mathbb{R}^3_I$ for a fixed $a = 0.9$. Gray denotes the region of possible values of L, E, and Q.

$$W(L_*, E_*) = \left.\frac{d^2R}{dr^2}\right|_{r=r_c} = 0. \tag{37}$$

Now we find the derivatives $\frac{dE}{dr_c}$ and $\frac{dL}{dr_c}$ for $Q = \text{const}$ on the bifurcation curves. Let us differentiate Eqs. (24) with respect to r_c, taking into account the fact that $E = E(r_c)$ and $L = L(r_c)$. Solving the resulting system, we find that

$$\frac{dE}{dr_c} = d^{-1}\left.\frac{\partial R}{\partial L}\frac{d^2R}{dr^2}\right|_{r=r_c}, \qquad \frac{dL}{dr_c} = -d^{-1}\left.\frac{\partial R}{\partial E}\frac{d^2R}{dr^2}\right|_{r=r_c},$$
$$d = \left.\left(\frac{\partial R}{\partial E}\frac{\partial^2 R}{\partial L \partial r} - \frac{\partial R}{\partial L}\frac{\partial^2 R}{\partial E \partial r}\right)\right|_{r=r_c}. \tag{38}$$

In relations (38), the partial derivatives of the function $R(r)$ denote differentiation with respect to the parameters L and E. From this it follows immediately that, when $E = E_*$ and $L = L_*$, these relations vanish; i.e., this point on the bifurcation curve is a cusp.

The value $r_c = r_*$ corresponding to the cusp separates the unstable critical trajectories $r_c < r_*$ $\left(\frac{d^2R}{dr^2} > 0\right)$ and the stable ones $r_c > r_*$ $(\frac{d^2R}{dr^2} < 0)$.

To obtain relations defining r_*, L_*, and E_*, we represent Eqs. (24) and (37) in the following form:

$$R - r\frac{dR}{dr} + \frac{r^2}{2}\frac{d^2R}{dr^2} = 3r_*^4(E_*^2 - 1) - Qa^2 + 2r_*^3 = 0,$$
$$\frac{1}{2}\frac{d^2R}{dr^2} = (a^2 + 6r_*^2)(E_*^2 - 1) + 6r_* - Q - L_*^2 = 0.$$

Taking into account the fact that $E_* > 0$, we find that

$$E_* = \frac{\sqrt{3r_*^4 - 2r_*^3 + Qa^2}}{r_*^2\sqrt{3}},$$
$$L_*^{\pm} = \pm\frac{\sqrt{Q(a^4 + 6a^2r_*^2 - 3r_*^4) + 2r_*^3(3r_*^2 - a^2)}}{r_*^2\sqrt{3}},$$

where the upper sign refers to L_*^+ and the lower sign refers to L_*^-. Next, we substitute both solutions into the first of relations (24) and, multiplying the resulting expressions, find an equation defining r_* in the following form:

$$\begin{aligned} G &= \frac{9r^3}{4}R(r_*)|_{L=L_c^+}R(r_*)|_{L=L_c^-} \\ &= 8Qa^2[r_*^3 + 2Qa^2][r_*(1 - a^2) + \Delta(r_*)(r_* - 1)] \\ &\quad + 24a^2r_*^4(1 - a^2)Q \\ &\quad + r_*^5[(\Delta(r_*) - 4(a^2 + r_*))^2 - 64a^2r_*] = 0. \end{aligned} \tag{39}$$

The curves $G(r_*, a) = 0$ for different fixed $Q \in [0, Q_c)$ are shown in Fig. 11, from which some conclusions can be drawn:

(a) The fixed values of Q and a correspond to two values of r_*. The smaller one corresponds to Eq. (34a) and the other one to Eq. (34b).

(b) r_* takes the minimal value if $Q = 0$. It corresponds to plane trajectories lying in the equatorial plane $\theta = \pi/2$. In this case, Eq. (39) simplifies and its solutions have the form

$$r_*^{\pm} = 3 + Z_2 \mp ((3 - Z_1)(3 + Z_1 + 2Z_2))^{1/2},$$
$$Z_1 = 1 + (1 - a^2)^{1/3}((1 + a)^{1/3} + (1 - a)^{1/3}),$$
$$Z_2 = (3a^2 + Z_1^2)^{1/2},$$

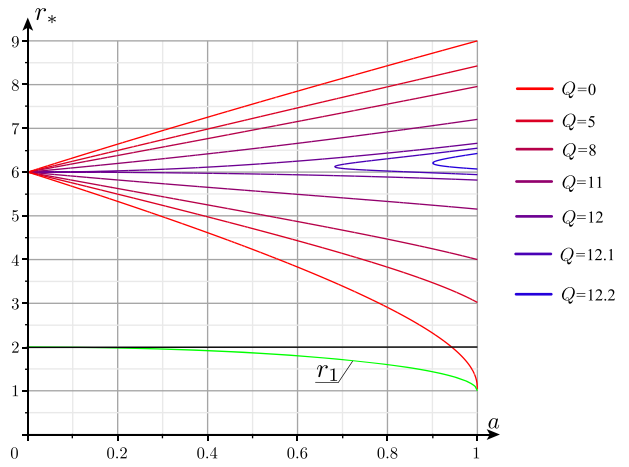

FIG. 11. Curves on the plane (r_*, a) which correspond to a cusp and are defined by Eq. (39) for different values of $Q < Q_c$. Green denotes the dependence $r_1(a)$.

where r_*^+ and r_*^- correspond to the curves (34a) and (34b), respectively. The quantity r_*^+ is called the ISCO since it describes the smallest radius for which the circular orbit is stable. As can be seen, for $a = 1$ we have $r_*^+ = r_+$.

(c) There are stable spherical trajectories $2 > r_c > r_*$ which lie in the ergosphere.

If $Q > Q_c$, then on the curves defined by relations (34) there are no critical points (see Fig. 10). In this case the lower bifurcation curve on the section $Q = \text{const}$ corresponds to stable spherical trajectories since on this curve $\frac{d^2R}{dr^2} < 0$, while the upper curve corresponds to unstable ones since $\frac{d^2R}{dr^2} > 0$.

E. A complete classification of integral submanifolds $\mathcal{M}_I^2$

Summing up the main results of the previous sections, we conclude that in the space of values of the first integrals $\mathbb{R}_I^3$ there are five bifurcation surfaces:

$$\Sigma_0^\theta, \qquad \Sigma_{\min}^\theta, \qquad \Sigma_0^r, \qquad \Sigma_\infty^r, \qquad \Sigma^t.$$

As they intersect, the type of the integral submanifold $\mathcal{M}_I^2$ changes. These surfaces divide the entire space $\mathbb{R}_I^3$ into regions in such a way that there exist seven different regions of values of the first integrals L, E, and Q for which motion is possible. In each of these regions the type of the integral submanifold $\mathcal{M}_I^2$ is the same.

Since the flat projection shows the structure of the 3D images of these regions very poorly, we will depict them using the sections formed by the intersection with the plane $Q = \text{const}$ (see Fig. 12). Since all types of the integral submanifolds $\mathcal{M}_I^2$ are shown in Fig. 12, we will not repeat these results here but instead will give only the necessary explanations.

Depending on the value of Q, the entire space $\mathbb{R}_I^3$ splits into three parts (layers):

$$D_1 = \{Q < 0\}, \quad D_2 = \{0 < Q < Q_c\}, \quad D_3 = \{Q_c < Q\},$$

in each of which the section formed by the intersection of the bifurcation diagram with the plane $Q = \text{const}$ looks similar. Before we proceed to the discussion of each of the parts, we make some general remarks. First, the planes Σ_∞^r and Σ^t are intersected by any section $Q = \text{const}$ along two straight lines which do not depend on the value of Q. Second, from the form of the latitudinal potential U_θ (see Figs. 3 and 4), it follows that

(a) for $L \neq 0$ there exists a neighborhood near the symmetry axis which the particle cannot enter (the case $L = 0$ requires a separate analysis; see Ref. [53]);

(b) if $Q < 0$ (i.e., in layer D_1), all particle trajectories do not intersect with the equatorial plane; and

(c) if $Q > 0$ (i.e., in layers D_2 and D_3), the region of possible particle motion always contains the equatorial plane.

It is important to keep in mind that all regions having the same color in Fig. 12 (i.e., those corresponding to the same type of $\mathcal{M}_I^2$) turn out to be *connected* in the three-dimensional space $\mathbb{R}_I^3$, even despite the fact that some of their sections formed by the intersection with the plane $Q = \text{const}$ are disconnected. Figure 13 shows a typical dependence of the functions $R(r)$ and $\Theta(\theta)$ in these regions and a projection of the corresponding integral submanifolds $\mathcal{M}_I^2$ onto the half plane (r, θ).

1. Part D_1 [see Fig. 12(a)]

If $Q < 0$, then there is only one region of possible motion. The section of this region is shown in Fig. 12(a). It is bounded by the surface $\Sigma_{\min}^\theta$, and the section formed by the intersection of this surface with the plane $Q = \text{const}$ consists of two hyperbolas intersecting with each other when $L = 0$.

As can be seen from Fig. 13, the motion of the particle occurs inside the spherical (more precisely, spheroidal) segment, and all trajectories, as they continue moving in forward time t, go to infinity $(r \to +\infty)$; as they move in backward time, they approach the horizon $(r \to r_+)$. There are no bounded trajectories for $Q < 0$, and the energy of the particle is always positive $(E > 0)$. Critical trajectories corresponding to the values of the integrals L, E, and Q on the bifurcation surface $\Sigma_{\min}^\theta$ are always unbounded and stable.

2. Part D_2 [see Fig. 12(b)]

The section formed by the intersection of the surface Σ_0^r with the plane $Q = \text{const}$ consists of two nonintersecting

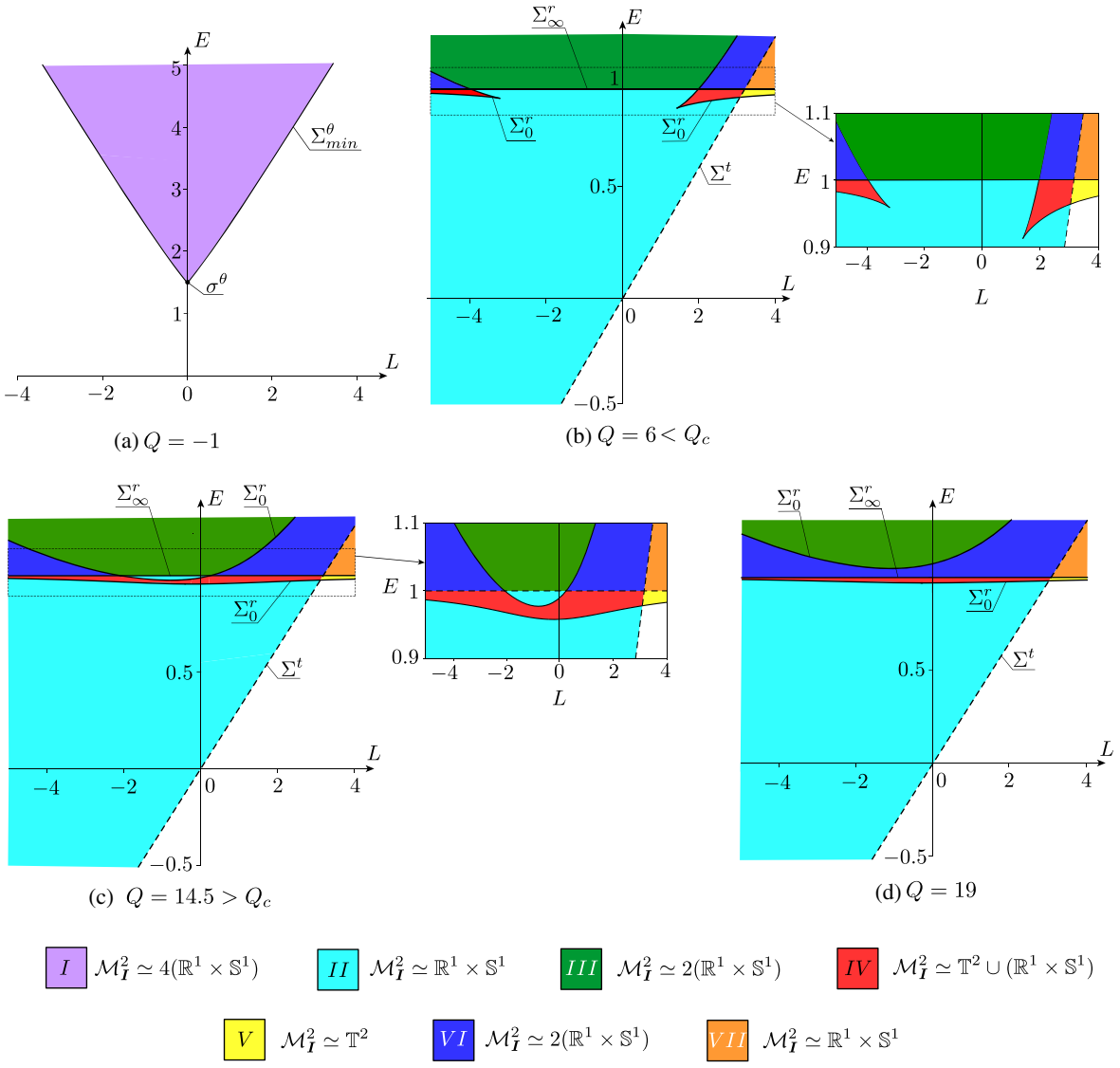

FIG. 12. Locations of regions with different numbers of connected components and their topological type on the plane (L, E) for different values of Q and for a fixed $a = 0.9$. The number in front of the brackets (if there is one) shows the number of identical connected components of the submanifold $\mathcal{M}^2_I$. The white regions correspond to nonphysical values of the integrals L and E with a fixed $Q = \text{const}$.

curves σ^+ and σ^-. For one of the curves, σ^-, the angular momentum $L \to -\infty$ as $r_c \to +\infty$, while for the other, σ^+, we have $L \to +\infty$ as $r_c \to +\infty$. On each of the curves, σ^- and σ^+, there is a cusp point, (L^-_*, E^-_*) and (L^+_*, E^+_*), respectively, which divides each curve into two smooth branches (at least of smoothness class C^1).

For the curve σ^- the following relations hold:

$$L \in (-\infty, L^-_*], \qquad L^-_* < 0,$$
$$E \in [E^-_*, +\infty), \qquad E^-_* < 1.$$

That is, this curve always lies to the left of the axis $L = 0$. One of the smooth branches of this curve for which the relation $E^-_* < E < 1$ is satisfied everywhere corresponds to stable critical solutions, and the other corresponds to unstable ones.

For the curve σ^+ the following relations are satisfied:

$$L \in (-\infty, L^+_*],$$
$$E \in [E^+_*, +\infty), \qquad E^-_* < 1,$$

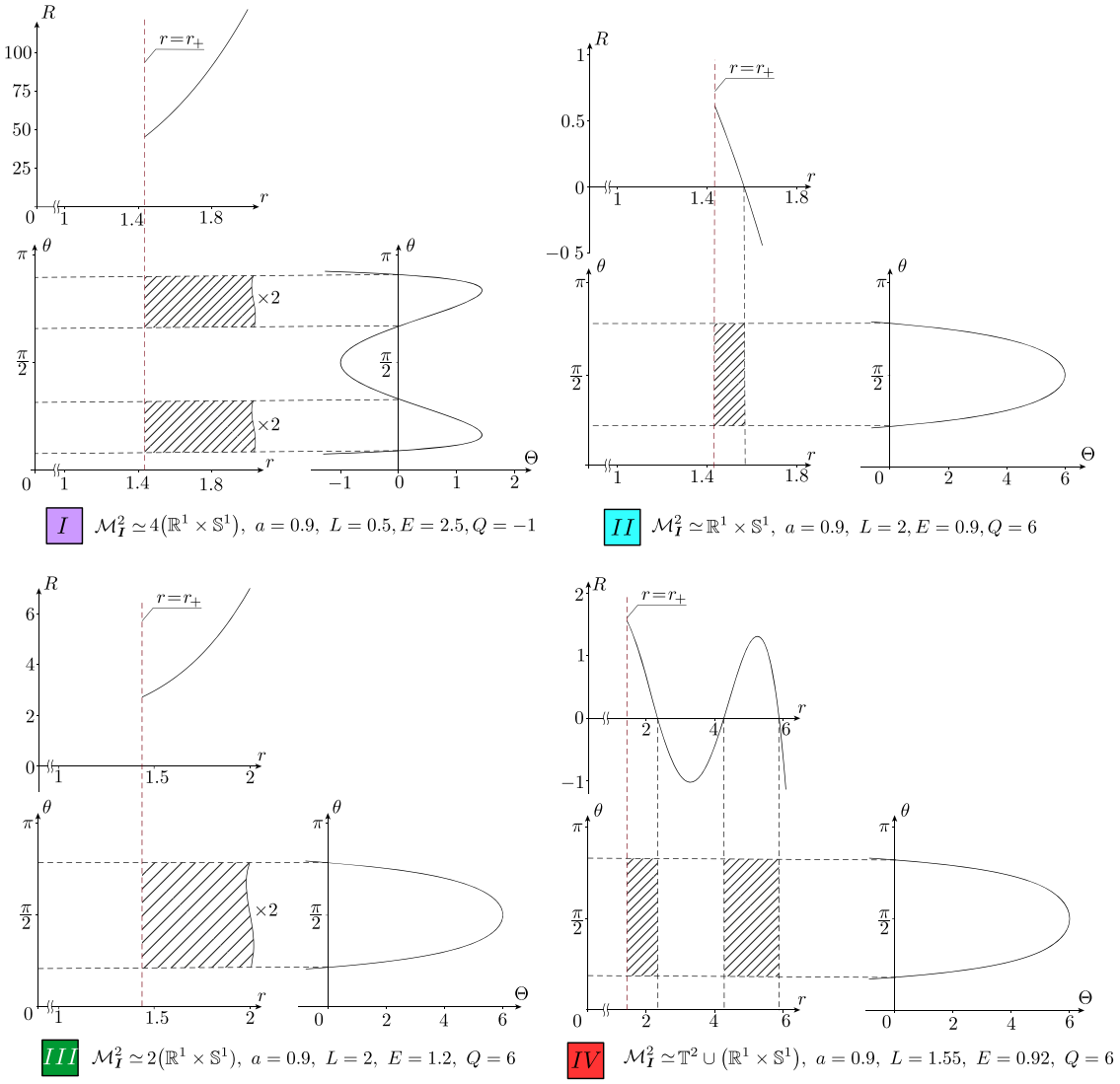

FIG. 13. Typical view of the functions $R(r)$ and $\Theta(\theta)$ and the projection of the corresponding integral submanifolds $\mathcal{M}^2_I$ onto the plane (r, θ).

and there is a value of $Q_* < Q_c$ such that for $Q < Q_*$ one has $L^+_* > 0$, and for $Q > Q_*$ one has $L^+_* < 0$; i.e., at some values of Q the curve σ_2 intersects with the axis $L = 0$. One of the smooth branches of this curve for which the relation $E^+_* < E < 1$ is satisfied also corresponds to stable critical solutions, and the other corresponds to unstable ones.

3. Part D_3 [see Figs. 12(c) and 12(d)]

The section formed by the intersection of the surface Σ^r_0 with the plane $Q = \text{const}$ also consists of a pair of nonintersecting curves σ_1 and σ_2. Both curves, σ_1 and σ_2, are smooth everywhere (at least of the smoothness class C^1) and for each of them one has $L \in (-\infty, +\infty)$.

For the curve σ_1 the relation $0 < E < 1$ always holds. All critical solutions corresponding to the values of the integrals on the curve σ_1 are stable.

For the second curve, σ_2, one has $E \in [E_{\min}, +\infty)$, and there is a Q_* such that for $Q_c < Q < Q_*$ one has $0 < E_{\min} < 1$, and for $Q > Q_*$ one has $E_{\min} > 1$. All critical solutions corresponding to the values of the integrals on σ_2 are unstable.

Thus, we see that in $\mathbb{R}^2_I$ there are only two regions, IV and V (both of them lie inside layers D_2 and D_3) for which there are compact integral submanifolds $\mathcal{M}^2_I$: two-dimensional tori. In the other regions, the integral submanifolds $\mathcal{M}^2_I$ are noncompact and diffeomorphic to two-dimensional cylinders (see Fig. 14). The difference between them (which results in $\mathbb{R}^3_I$ splitting into corresponding regions) lies in the behavior of the trajectories on this submanifold as $t \to +\infty$ and $t \to -\infty$.

(a) In regions I and III all trajectories on $\mathcal{M}^2_I$ either "start" as $t \to -\infty$ at infinity ($r \to +\infty$) and "end" as $t \to +\infty$ at the horizon ($r \to r_+$) or, conversely, either start

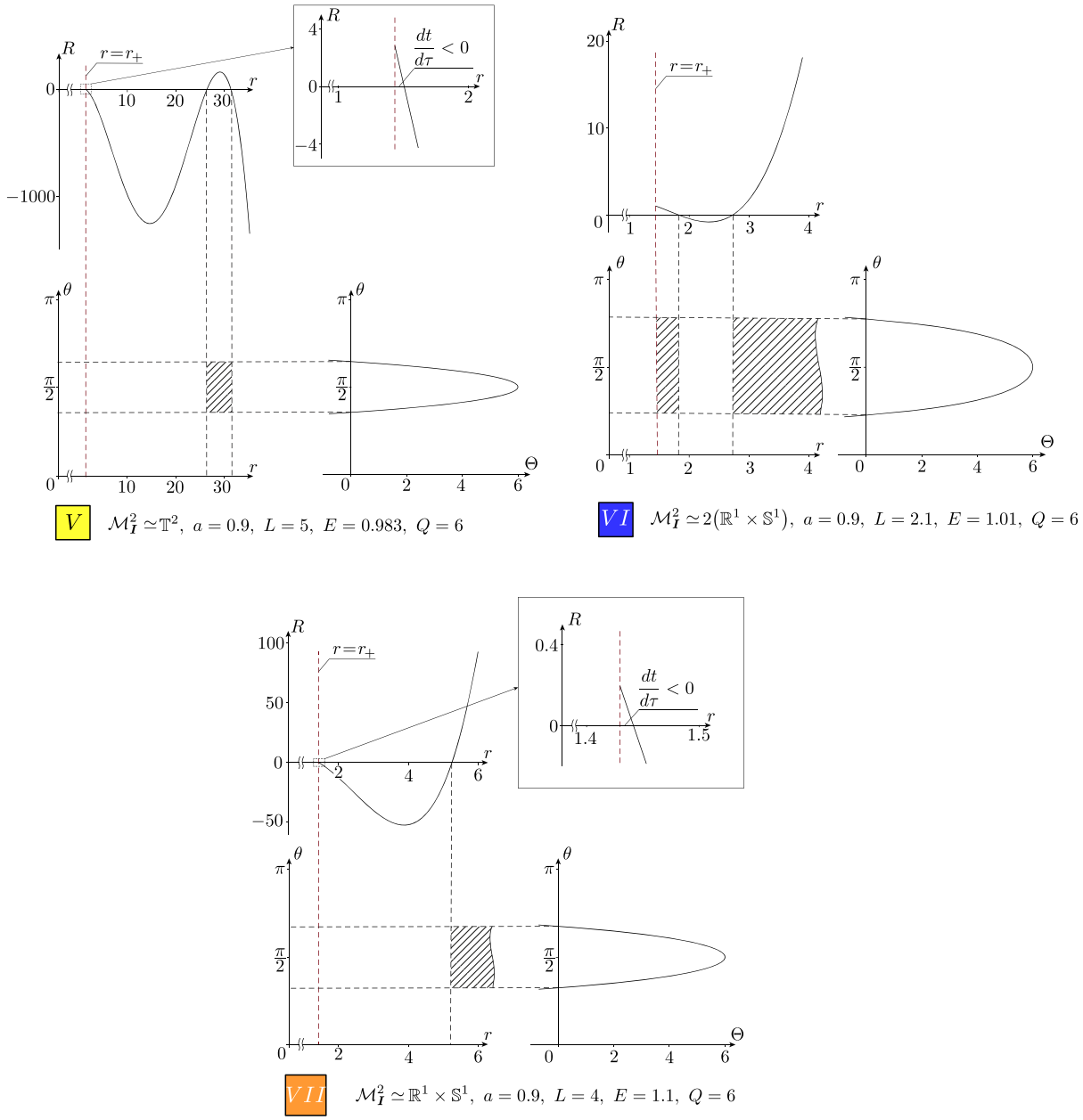

FIG. 14. Typical view of the functions $R(r)$ and $\Theta(\theta)$ and the projection of the corresponding integral submanifolds $\mathcal{M}^2_I$ onto the plane (r, θ).

at the horizon and end at ∞; in this paper, we call such an $\mathcal{M}^2_I$ the "horizon/infinity."

(b) In region II all trajectories on $\mathcal{M}^2_I$ are of the type "infinity/infinity."

(c) In region VI there are two types of integral submanifolds: "horizon/horizon" and horizon/infinity.

IV. CRITICAL TRAJECTORIES OF THE KERR METRIC

We now consider in more detail the (most interesting) *critical trajectories* of the system, i.e., particle motions for which the integrals of motion L, E, and Q lie on the bifurcation surfaces Σ^r, Σ^θ. A characteristic feature of these trajectories is that the dimension of the corresponding integral submanifold is one less—namely, for the reduced system (15) the dimension is 1, and for the complete system (11) the dimension is 2.

A. Trajectories in the equatorial plane

Let the value of the Carter integral be zero ($Q = 0$). Then it follows from the analysis of of the latitudinal motion (see Sec. III C and Fig. 17) that there are

trajectories lying in the equatorial plane $\theta = \pi/2$, and that all of them are critical (since in this case the latitudinal potential has a critical point).

According to the results of Sec. III, the equatorial invariant plane $\theta = \pi/2$ is stable under the condition

$$a^2(E^2-1) - L^2 < 0, \tag{40}$$

and unstable otherwise. The equation governing the evolution of the radial coordinates for plane trajectories has the form

$$\begin{aligned} \frac{dr}{d\tau} &= \pm\frac{1}{r^2}\sqrt{R(r)}, \\ R(r) &= r[(E^2-1)r^3 + 2r^2 \\ &\quad + (a^2(E^2-1) - L^2)r + 2(L-aE)^2]. \end{aligned} \tag{41}$$

We represent Eqs. (20) in the form

$$\frac{d\varphi}{d\tau} = \frac{2aE + L(r-2)}{r\Delta(r)}, \quad \frac{dt}{d\tau} = E + \frac{2}{r\Delta(r)}(E(r^2+a^2) - aL).$$

A bifurcation diagram for this case is shown in Fig. 15. In fact, this is a section formed by the intersection of the general diagram (see Sec. III) with the plane $Q = 0$. Nevertheless, the interpretation of the bifurcation curves differs somewhat from the preceding in that, as noted above, the curve $\Sigma^\theta_+ \cup \Sigma^\theta_-$ divides the regions of stability and instability of the planar motion. Also, the curves Σ^r_+ and Σ^r_- correspond to fixed points (and not to periodic solutions) of the reduced system (15), i.e., *critical circular trajectories* of the initial system (11). The curve Σ^r_∞ also corresponds to a nonlocal bifurcation such that, when it is intersected with (toward an increase in E), the particle can leave the neighborhood of the horizon. The curve Σ^t bounds, as above, the region of possible values of the integrals for motions reaching the ergosphere.

For each fixed value $L = L_0$ the system (41) defines on the plane $(r, \frac{dr}{d\tau})$, $r > r_+$, a set of trajectories corresponding to different values of the integral E. They form the so-called phase portrait of a reduced system with a fixed angular momentum. From the form of the bifurcation diagram in Fig. 15 it follows that there are four critical values of the integral of the angular momentum L at which the phase portrait will not qualitatively change, as indicated next.

(a) L^c_-, L^c_+: values of L which correspond to cusp points on the curves Σ^r_- and Σ^r_+.

(b) L^e_-, L^e_+: values of L at which the curves Σ^r_- and Σ^r_+ intersect with the straight line $E = 1$.

Depending on the choice of L, three types of phase portraits of the reduced system are possible (Fig. 16).

Remark 9.—We see that the region of unstable planar motions which is given by inequality (40) (i.e., the region bounded by the curve $\Sigma^\theta_{\min}$) is very small [see Figs. 15 and 17(a)]. If L and E are chosen in the region $a^2(E^2-1) - L^2 > 0$, then, in addition to plane trajectories,

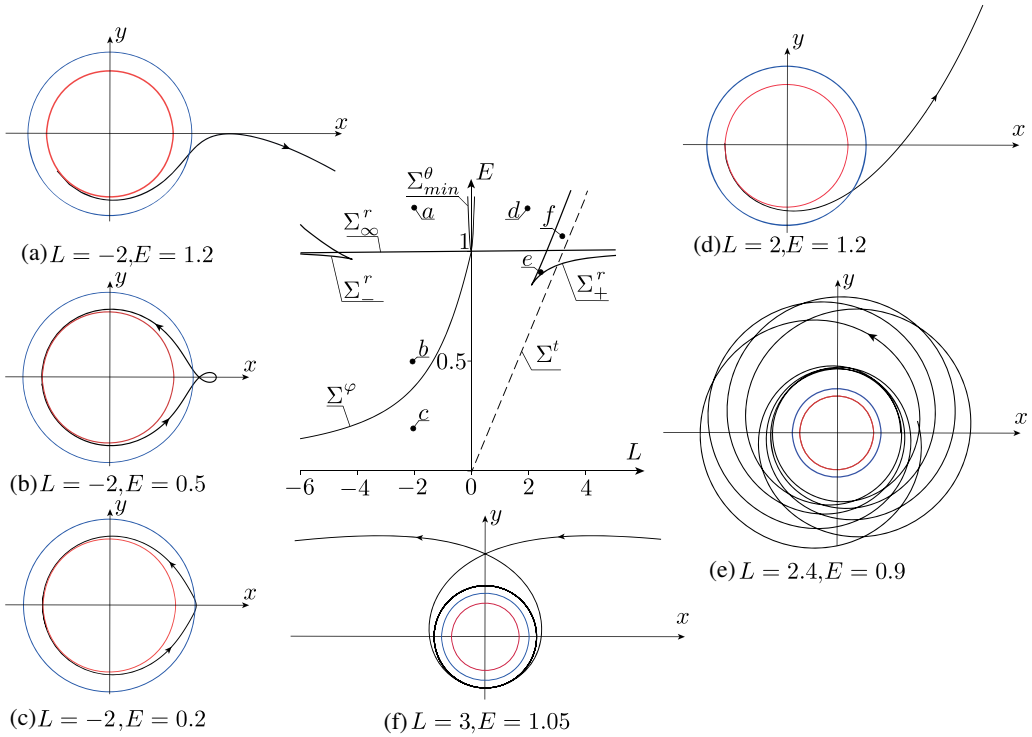

FIG. 15. Typical view of the trajectories of a particle with $a = 0.9$ for different values of the integrals L and E, where red denotes the event horizon h and blue denotes the boundary of the ergosphere s.

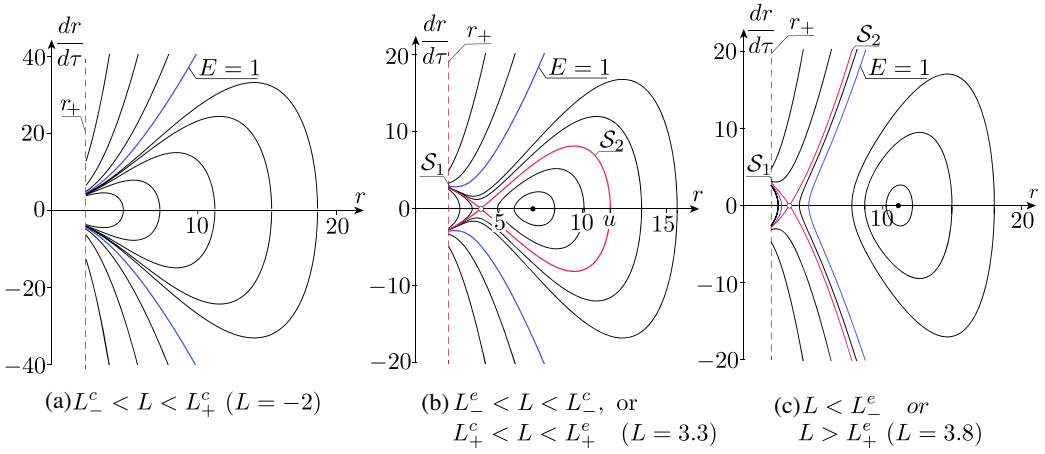

FIG. 16. Three possible types of phase portraits of a reduced system for a fixed value of L ($a = 0.3$).

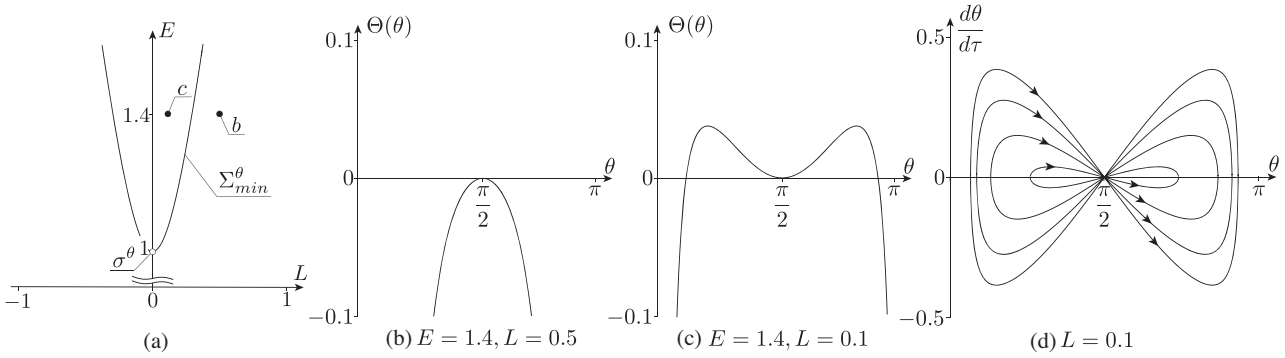

FIG. 17. (a) Shape of $\Sigma_{\pm}^{(\theta)}$ on the half plane $\mathbb{R}^2_{L,E}$ for a fixed $a = 0.3$, (b),(c) the behavior of the function $\Theta(\theta)$ in different regions, and (d) a typical view of a trajectory on the plane $(\theta, \frac{d\theta}{d\tau})$ for a fixed value of L and different values of E.

there are trajectories that do not lie entirely in the equatorial plane [see Fig. 17(d)]. As $\tau \to \pm\infty$, the above-mentioned trajectories tend asymptotically to the equatorial plane (see Fig. 17). After explicit integration of the equation for the angle θ after the time rescaling (19), we obtain the following relations for the trajectories:

$$\cos\theta(u) = \pm\left(1 - \frac{L^2}{a^2(E^2-1)}\right)^{1/2}$$
$$\cosh^{-1}\left[Lu\left(\frac{a^2(E^2-1)}{L^2} - 1\right)^{1/2} + C\right], \quad C = \text{const}.$$

The curve $a^2(E^2-1) - L^2 = 0$ lies in region III, which contains the unbounded trajectories reaching the event horizon $r = r_+$. Therefore, $u \in (0, u_0)$, where u_0 is the time it takes for the trajectory to reach the event horizon $r = r_+$. In other words, these trajectories can reach the event horizon before they approach the equatorial plane.

Consider the critical circular trajectories $r = r_c = \text{const}$. For them the values of the integrals L and E are defined by relations (35). This yields the following expression for the angular velocity:

$$\omega_{\pm} = \frac{d\varphi}{dt} = \frac{1}{a \pm r_c^{3/2}}, \tag{42}$$

where the upper sign refers to Σ^r_+ and the lower sign refers to Σ^r_-. Since $r_c > 1 > a$, we see that if $(L, E) \in \Sigma^r_-$ the particle rotates in the opposite direction of the rotation of the celestial body, while if $(L, E) \in \Sigma^r_+$ the direction of rotation of the particle is the same as that of the celestial body.

In the general case, the direction of rotation for the plane trajectories can change since $\frac{d\varphi}{d\tau}$ vanishes for some value of the radial coordinate.

Proposition 3.—If the trajectory changes the direction of rotation, then the integrals L and E satisfy the inequalities

$$L < 0, \qquad E > 0, \qquad a(E^2-1) - EL > 0. \tag{43}$$

The value of the radial coordinate $r = r_\varphi$ corresponding to the change in the direction of rotation is defined by the relation $\frac{d\varphi}{d\tau} = 0$. Hence, we obtain

$$r_\varphi = 2\left(1 - \frac{aE}{L}\right) > r_+. \tag{44}$$

Also, the following condition must be satisfied,

$$R(r_\varphi) = \frac{4\Delta(r_\varphi)(aE - L)^2}{L^4}[a(E^2 - 1) - EL] \geq 0,$$

and it is equivalent to the inequality

$$a(E^2 - 1) - EL \geq 0. \tag{45}$$

Let $E < 0$. Then, in view of Eq. (14), inequality (45) can be represented as

$$-\frac{ar_+^2 L^2}{(r_+^2 + a^2)^2} - a > 0.$$

As we see, on the left-hand side the quantities take only negative values, which gives a contradiction; hence, $E > 0$. Taking this into account, we represent condition (45) as

$$E \geq \frac{L + \sqrt{L^2 + 4a^2}}{2a}.$$

Then relation (44) can be rewritten as

$$-\sqrt{1 - a^2} - \frac{\sqrt{L^2 + 4a^2}}{L} > 0.$$

It can be satisfied only if $L < 0$. Therefore, inequalities (43) must be satisfied.

Thus, the following additional curve arises on the plane (L, E),

$$\Sigma^\varphi = \{(L, E) | E = E_\varphi, L < 0\}, \qquad E_\varphi = \frac{L + \sqrt{L^2 + 4a^2}}{2a},$$

above which lie the values of the integrals L and E for which the trajectory changes the direction of rotation.

A typical view of trajectories from different regions on the plane of the integrals (L, E) is shown in Fig. 15. Below we briefly describe them.

(a) If $L < 0$, $E < E_\varphi$ [see Fig. 15(c)] or $L > 0$ [see Fig. 15(d)], then the direction of rotation along the entire trajectory is the same as that of the celestial body $\frac{d\varphi}{d\tau} > 0$.

(b) Let the values of the integrals L and E lie in the region bounded by the curve Σ_-^r. Then, in addition to the trajectories for which $r \in (r_+, r_u^{(1)}]$, there are also bounded trajectories $r \in [r_u^{(2)}, r_u^{(3)}]$ if $E < 1$ and unbounded trajectories $r \in [r_u^{(2)}, +\infty)$ if $E > 1$. Here $r_u^{(i)}$, $i = 1, 2, 3$ are the zeros of the polynomial $R(r)$. For these trajectories (i.e., if $r > r_u^{(2)}$), the direction of rotation never coincides with that of the celestial body $\frac{d\varphi}{d\tau} < 0$ (see Fig. 13). To show this, it suffices to note that, according to Eq. (42), for $r = r_c$ we have $\frac{d\varphi}{d\tau} \neq 0$.

(c) The direction of rotation changes for the trajectories [see Figs. 15(a) and 15(b)] for which the values of the integrals lie in the region $L < 0$, $E > E_\varphi$. In this case, the values are in the region bounded by the curve Σ_-^r at the initial time $r \in (r_+, r_u^{(1)}]$.

1. Separatrices

As can be seen in Fig. 16, if $L < L_-^e$ or $L > L_+^e$, then the phase portrait of the system has a fixed saddle point corresponding to the unstable circular orbit $r = r_c$. Adjacent to this point are asymptotic trajectories—*separatrices* for which the solution is given in terms of elementary functions (see also Ref. [27]).

Remark 10.—Under a nonintegrable perturbation, it is usually in the neighborhood of a separatrix that the most considerable stochastic layer arises. In addition, an explicit solution for the separatrix is used, for example, when calculating the Melnikov integral.

To obtain the corresponding solution, we substitute the values of the integrals L and E on the curves Σ_+^r and Σ_-^r from relations (35) into the function $R(r)$ and represent it as

$$R(r) = \frac{4br}{r_c}\frac{r - r_a}{r_c - r_a}(r - r_c)^2,$$
$$b = \frac{r_c}{2} - \frac{3}{4}r_c^2(1 - E_\pm^2), \qquad r_a = \frac{2r_c(a \mp r_c^{1/2})^2}{r_c^2 - (a \mp 2r_c^{1/2})^2}. \tag{46}$$

From the results of Sec. III D for the stability of critical solutions, it follows that in the case of an unstable fixed point one has $r_c < r_*^\pm$, and it can be shown that the following inequalities hold:

$$0 < b,$$
$$0 < r_c < r_a \quad \text{for } E < 1,$$
$$r_a < 0 \quad \text{for } E > 1.$$

Furthermore, rescaling time as in Eq. (19), we obtain

$$d\tau = (\rho(r, \theta)du)|_{\theta = \pi/2} = r^2 du.$$

As seen in Fig. 16, if $r_+ < r < r_c$, there are a pair of separatrices S_1^u and S_1^s which intersect with the event horizon r_+. Integrating Eq. (41), we find for them the expression

$$r(u) = r_c \frac{\sinh^2(\sqrt{b}u)}{\cosh^2(\sqrt{b}u) - r_c/r_a}.$$

The stable separatrix S_1^s corresponds to $u \in [u_+, +\infty)$ and the unstable separatrix S_1^u corresponds to $u \in (-\infty, -u_+)$, where u_+ is the positive root of the equation $r(u_+) = r_+$.

Remark 11.—Strictly speaking, S_1^u and S_1^s are not different separatrices but rather two parts of the same homoclinic separatrix, which emanates from a fixed point as $u \to -\infty$, dips under the event horizon, and returns to the fixed point as $u \to +\infty$.

Again coming back to the phase portrait in Fig. 16, we see that if $L_-^e < L < L_-^c$ or $L_+^c < L < L_-^e$, i.e., $E < 1$, then a (homoclinic) separatrix S_2 which encloses some region around a stable fixed point [Fig. 16(b)] emanates from the fixed saddle point. In this case, $r_c < r \le r_a$ and is given by

$$r(u) = r_c \frac{\cosh^2(\sqrt{b}u)}{\sinh^2(\sqrt{b}u) + r_c/r_a}.$$

As we see, this solution bounds the finite trajectories for which the radial coordinate changes periodically with time. Consequently, for finite trajectories the radial coordinate does not exceed r_a in this case.

If $E > 1$, then the phase portrait has a pair of separatrices S_2^u and S_2^s which go to infinity ($r \to +\infty$). In this case $r_a < 0$, and an explicit solution is given by the expression

$$r(u) = r_c \frac{\cosh^2(\sqrt{b}u)}{\sinh^2(\sqrt{b}u) - r_c/|r_a|}, \tag{47}$$

where for S_2^s and S_2^u we have $u \in (u_+, +\infty)$ and $u \in (-\infty, -u_+)$, respectively, with u_+ being the positive root of the denominator in Eq. (47).

In addition to the above-mentioned separatrices $\mathcal{S}_1$ and $\mathcal{S}_2$, there is a special case where the solution is expressed in terms of elementary functions. Indeed, let $(L, E) \in \Sigma_+^r$ and $r_c > r_+^*$ or $(L, E) \in \Sigma_-^r$ and $r_c > r_-^*$. Then, except for the stable equilibrium point $r = r_c$, these values of the integrals also correspond to the bounded trajectory starting and ending at the event horizon $r = r_+$. For this trajectory the function $R(r)$ is also represented as Eq. (46), but in this case $b < 0$ and $0 < r_a < r_c$. After explicit integration of the equation for the radial coordinate, we obtain

$$r(u) = r_c \frac{\sin^2(\sqrt{|b|}u)}{r_c/r_a - \cos^2(\sqrt{|b|}u)}, \quad u \in (-u_+, u_+),$$

where u_+ is the positive root of the equation $r(u) = r_+$.

2. Invariant tori, rotation numbers, and resonances

Assume that the values of the integrals L and E lie in a region bounded by the curves $\Sigma_\pm^r$ and $E < 1$. According to the results of Sec. III D, three roots of the polynomial $R(r)$ lie on the interval $(r_+, +\infty)$ in this case:

$$R(r) = (E^2 - 1)(r - r_u^{(1)})(r - r_u^{(2)})(r - r_u^{(3)})r,$$
$$r_+ < r_u^{(1)} < r_u^{(2)} < r_u^{(3)},$$

and the segment $[r_u^{(2)}, r_u^{(3)}]$ defines the bounded trajectories [see Figs. 6(b), 16(b), and 16(c)].

Let $r \in [r_u^{(2)}, r_u^{(3)}]$. Then, each time the turning point $r_u^{(2)}$ or $r_u^{(3)}$ is reached, one should change the sign in Eq. (41) for $\frac{dr}{d\tau}$. To avoid this difficulty, we transform to the angle variable $\psi \in (0, 2\pi]$:

$$r = \frac{r_u^{(3)} - r_u^{(2)}}{2}\cos\psi + \frac{r_u^{(3)} + r_u^{(2)}}{2}.$$

We finally obtain equations governing the motion on invariant tori $\mathbb{T}^2 = \{(\psi, \varphi) \bmod 2\pi\}$ in phase space in the following form:

$$\frac{d\psi}{du} = d\sqrt{(\Gamma_1 + \cos\psi)(\Gamma_2 + \cos\psi)},$$
$$\frac{d\varphi}{du} = \Phi(\psi) = r\frac{2aE + L(r-2)}{\Delta(r)}\bigg|_{r=r(\psi)},$$
$$d = \frac{\sqrt{1-E^2}}{2}(r_u^{(3)} - r_u^{(2)}), \qquad \Gamma_1 = \frac{r_u^{(2)} + r_u^{(3)}}{r_u^{(3)} - r_u^{(2)}} > 1,$$
$$\Gamma_2 = \frac{r_u^{(2)} + r_u^{(3)} - 2r_u^{(1)}}{r_u^{(3)} - r_u^{(2)}} > 1. \tag{48}$$

As can be seen, the radicand on the first line of Eqs. (48) does not vanish.

The system of Eqs. (48), which governs the evolution of the angles ψ and φ, defines a vector field on the torus $\mathbb{T}^2$ without fixed points. It is the rotation number that allows one to classify the trajectories on $\mathbb{T}^2$ depending on the parameters. In this case the rotation number can be represented as

$$\rho_{L,E} = 2\pi d\left[\int_0^{2\pi} \frac{\Phi(\psi)d\psi}{\sqrt{(\Gamma_1 + \cos\psi)(\Gamma_2 + \cos\psi)}}\right]^{-1}.$$

If $\rho_{L,E}$ takes a rational value, then all trajectories on the corresponding invariant torus $\mathbb{T}^2$ with given values of L and E are periodic. If $\rho_{L,E}$ takes an irrational value, then the trajectories on the torus $\mathbb{T}^2$ are quasiperiodic. The curves on the plane L, E which correspond to the rational values of the rotation number equal to $1/3$, $1/2$, and $2/3$ are shown in Fig. 18.

B. Spherical trajectories

Let us consider critical trajectories $r = r_c = \text{const}$ which do not lie entirely in the equatorial plane. For an external

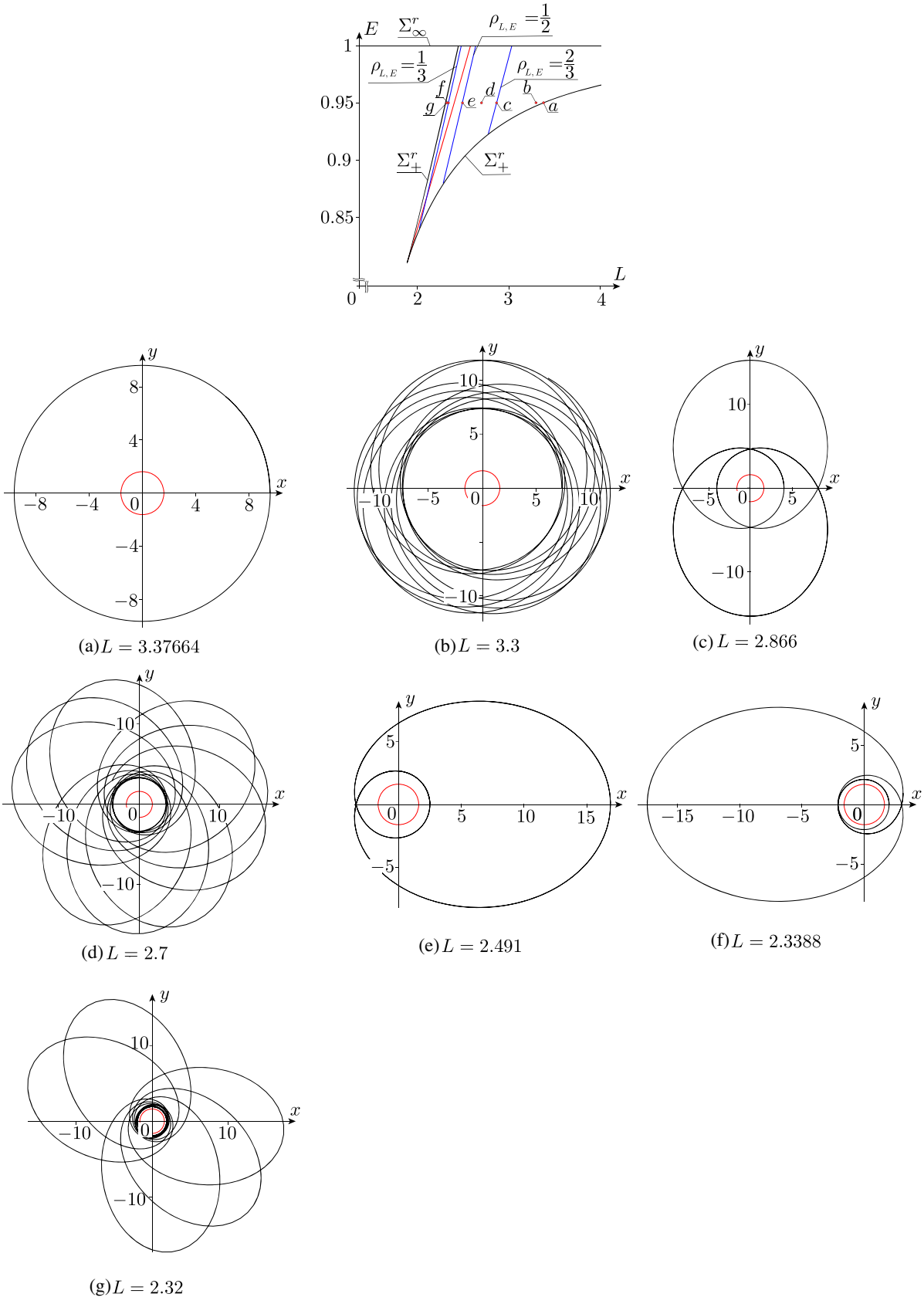

FIG. 18. Curves for the fixed $a = 0.95$ on the plane L, E which correspond to the rational values of the rotation number $\rho_{\varphi/r}$, and the trajectories in the equatorial plane for the fixed $E = 0.95$ and different L. Red denotes the curve for which $r_u^{(2)} = 2$.

fixed observer the surface $r = \text{const}$ is diffeomorphic to a sphere. Therefore, these critical trajectories are called *spherical*. To visualize them in the three-dimensional space, we will use the coordinates (3), in which the surface $r = \text{const}$ is a spheroid.

In the space of the first integrals, $\mathbb{R}^3_I$, spherical critical trajectories correspond to the bifurcation surface $\Sigma^r_0 = \Sigma^r_+ \cup \Sigma^r_-$ (see Fig. 10), which in our case (see Sec. III D) is parametrized by the quantities r_c and Q ($Q > 0$).

Next, we consider only stable spherical trajectories for which $E < 1$. In this case, the corresponding part of the surface Σ^r_0 is uniquely projected onto the half plane of the integrals $\mathbb{R}^2 = \{(L, Q) | Q > 0\}$ (see Fig. 10).

For the reduced system (15) the spherical critical trajectories define periodic solutions, while in the phase space of the initial system (11) they correspond to trajectories on the two-dimensional invariant tori $\mathbb{T}^2$. To obtain a flow on the invariant tori, we define their parametrization using suitable angular coordinates. One of the coordinates is the azimuthal angle of the particle φ, and the other angle variable ψ with $L \neq 0$ (the case $L = 0$ is analyzed in detail in, for example, [53]) can be determined by making the change of variable

$$\cos\theta = A\sin\psi,$$
$$A = \left(\frac{1}{2} + \frac{Q + L^2}{2a^2(1-E^2)} - \sqrt{\left(\frac{1}{2} - \frac{Q + L^2}{2a^2(1-E^2)}\right)^2 + \frac{L^2}{a^2(1-E^2)}}\right)^{1/2} < 1,$$

where A is the amplitude of the quantity $\cos\theta$ for a critical solution with a given value of the integrals L, E, and Q which is always smaller than unity for $L \neq 0$. Using Eqs. (18) and (20), we find that in the new variables the flow on the invariant tori $\mathbb{T}^2$ can be represented as

$$\frac{d\psi}{du} = a\sqrt{(1-E^2)(B^2 - A^2\sin^2\psi)},$$
$$\frac{d\varphi}{du} = \beta + \frac{L}{1 - A^2\sin^2\psi},$$
$$\beta = \frac{a}{\Delta(r_c)}(2Er_c - aL) = \text{const},$$
$$B = \left(\frac{1}{2} + \frac{Q + L^2}{2a^2(1-E^2)} + \sqrt{\left(\frac{1}{2} - \frac{Q + L^2}{2a^2(1-E^2)}\right)^2 + \frac{L^2}{a^2(1-E^2)}}\right)^{1/2}, \quad (49)$$

where $0 < A < 1 < B$.

According to relations (34), the values of the integrals for spherical trajectories with $r_c \gg 1$ can be represented as

$$L = \pm\sqrt{r_c} + O\left(\frac{1}{\sqrt{r_c}}\right), \qquad E = 1 - \frac{1}{2r_c} + O\left(\frac{1}{r_c^2}\right),$$

where the upper sign refers to Σ_+ and the lower sign refers to Σ_-. Therefore, for the amplitude of the angular deviation of the trajectory $\cos\theta$ we obtain

$$A = \frac{Q}{r_c} + O\left(\frac{1}{r_c^2}\right).$$

Thus, the angular deviation of the critical spherical trajectories from the equatorial plane tends to zero as $r_c \to +\infty$.

1. Pro- and retrograde trajectories (co- and counterrotating orbits)

We recall that in the case of the Schwarzschild metric the azimuthal angle φ changes monotonically with time (for both critical and general trajectories) [16]. We show that if $L < 0$, then there are spherical trajectories for which the direction of rotation about the symmetry axis changes.

Indeed, according to Eq. (49), the rate of change of the azimuthal angle, $\frac{d\varphi}{du}$, oscillates between the values

$$\beta + \frac{L}{1 - A^2} \quad \text{and} \quad \beta + L. \quad (50)$$

For $L > 0$ both these quantities are positive, while for $L < 0$ they may have different signs such that the trajectory becomes pro- and retrograde. The boundary of the existence region of these trajectories is found using the condition that the largest of the values (50) with $L < 0$ vanishes, i.e., $\beta + L = 0$. From this we find that

$$E = \frac{(2 - r_c)L}{2a}.$$

Next, substituting the resulting value of energy into Eq. (24) and solving the system thus obtained for L and Q, we obtain the following curve:

$$\Sigma^\varphi = \left\{(L, Q) | L = -\frac{2}{\sqrt{r_c(r_c - 3)}}, \; Q = \frac{r_c^2}{r_c - 3}, r_c \in (r_*, +\infty)\right\},$$

where r_* is the root of Eq. (39).

Thus, if the values of the integrals for the spherical trajectories lie in the region $L < 0$ to the right of the curve Σ^φ, then the function $\frac{d\varphi}{dt}$ has zeros (see Fig. 19).

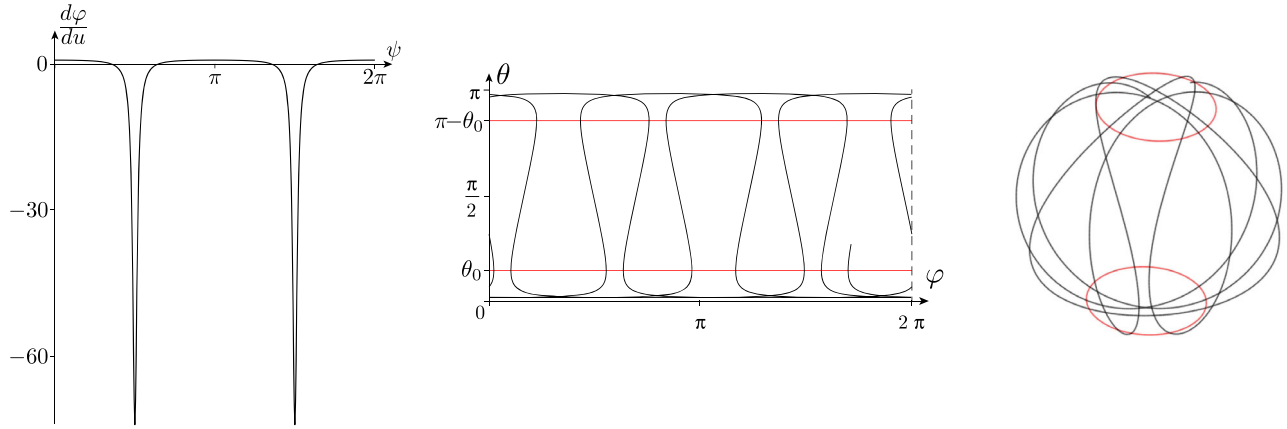

FIG. 19. Dependence of $\frac{d\varphi}{du}$ on ψ and a typical view of a trajectory on the plane (φ,θ) and in the coordinates (3) in the case where the function $\frac{d\varphi}{du}$ has zeros for the fixed values $a=0.95$, $Q=15$, $L=-0.2$, $r_c=3.6313$, and $E=0.9936$.

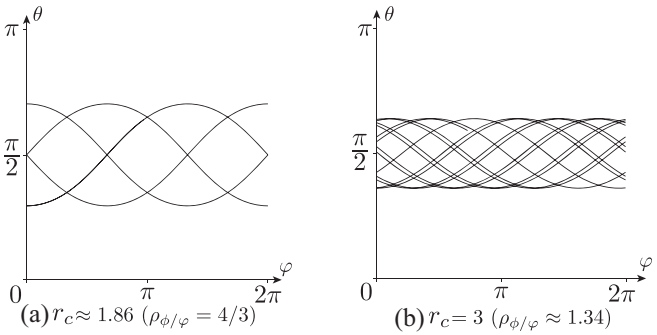

FIG. 20. Trajectory on the plane (φ,θ) for the fixed values $a=0.95$, $L=1.859$, $Q=2$, and $E=0.871$ and for different r_c.

2. Rotation number and resonances

The rotation number for the system (49) is found explicitly to be

$$\rho_{L,Q}=\frac{1}{2\pi a\sqrt{1-E^2}}\int_0^{2\pi}\left(\beta+\frac{L}{1-A^2\sin^2\phi}\right)\times(B^2-A^2\sin^2\phi)^{-1/2}d\phi=\frac{2L\Pi(A^2,\frac{A}{B})+2\beta K(\frac{A}{B})}{a\pi B\sqrt{1-E^2}},$$

where the following complete elliptic integrals are defined:

$$K(k)=\int_0^{\pi/2}\frac{dx}{\sqrt{1-k^2\sin^2 x}},$$
$$\Pi(n,k)=\int_0^{\pi/2}\frac{dx}{(1-n\sin^2 x)\sqrt{1-k^2\sin^2 x}}.$$

A typical view of a trajectory for which $\rho_{L,Q}$ takes rational and irrational values is shown in Fig. 20. The dependence of the rotation number $\rho_{L,Q}$ on L is shown in Fig. 21. As we see, the rotation number $\rho_{L,Q}$ has a discontinuity for $L=0$ (see also Ref. [21]).

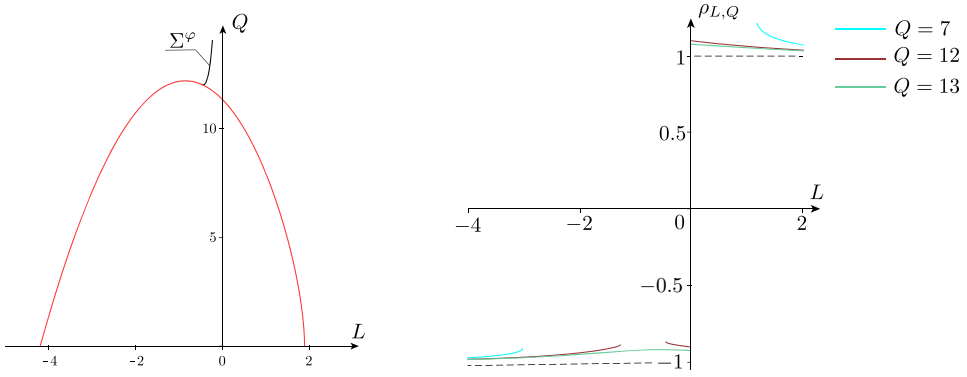

FIG. 21. Curve Σ^φ, where red denotes the boundary of stable spherical trajectories on the plane (L,Q), and dependence of the rotation number $\rho_{L,Q}$ on L for a fixed Q.

ACKNOWLEDGMENTS

Work pertaining to Secs. II and III was performed at the Ural Mathematical Center (Agreement No. 075-02-2022-889). The work in Sec. IV was carried out within the framework of the state assignment of the Ministry of Education and Science of Russia (Grant No. FEWS-2020-0009). The authors express their gratitude to S. V. Bolotin, V. V. Kozlov, and A. P. Veselov for the fruitful discussions and useful comments.

[1] S. Smale, Inventiones Mathematicae **10**, 305 (1970).
[2] V. M. Alekseev, Biulleten **10**, 241 (1965).
[3] H. Waalkens, H. R. Dullin, and P. H. Richter, Physica (Amsterdam) **196D**, 265 (2004).
[4] A. V. Bolsinov, A. V. Borisov, and I. S. Mamaev, Russ. Math. Surv. **65**, 259 (2010).
[5] T. Pogosian and M. Kharlamov, J. Appl. Math. Mech. **43**, 452 (1979).
[6] O. P. Krivenko, K. A. Pyragas, and I. T. Zhuk, Astrophys. Space Sci. **40**, 39 (1976).
[7] J. E. Marsden *et al.*, *Lectures on Mechanics*, Vol. 174 (Cambridge University Press, Cambridge, England, 1992).
[8] S. Pekarsky and J. E. Marsden, J. Math. Phys. (N.Y.) **39**, 5894 (1998).
[9] A. Borisov and V. Lebedev, Reg. Chaotic Dyn. **3**, 99 (1998).
[10] A. Bolsinov and A. Fomenko, *Integrable Hamiltonian Systems* (CRC Press, Boca Raton, 2004).
[11] L. M. Lerman and Y. L. Umanskii, Russ. Acad. Sci. Sb. Math. **77**, 511 (1994).
[12] A. V. Bolsinov, A. V. Borisov, and I. S. Mamaev, Reg. Chaotic Dyn. **17**, 451 (2012).
[13] D. V. Treshchev, Mathematical notes of the Academy of Sciences of the USSR **50**, 1067 (1991).
[14] B. Carter, Phys. Rev. **174**, 1559 (1968).
[15] J. Stewart and M. Walker, in *Springer Tracts in Modern Physics* (Springer, Berlin, 1973), pp. 69–115.
[16] S. Chandrasekhar, *The Mathematical Theory of Black Holes* (Oxford University Press, New York, 1983).
[17] N. A. Sharp, Gen. Relativ. Gravit. **10**, 659 (1979).
[18] J. M. Bardeen, W. H. Press, and S. A. Teukolsky, Astrophys. J. **178**, 347 (1972).
[19] J. Bicák and Z. Stuchlík, Bull. Astron. Inst. Czech. **27**, 129 (1976).
[20] O. P. Krivenko, K. A. Pyragas, and I. T. Zhuk, Astrophys. Space Sci. **40**, 39 (1976).
[21] D. C. Wilkins, Phys. Rev. D **5**, 814 (1972).
[22] E. Teo, Gen. Relativ. Gravit. **53**, 10 (2021).
[23] R. Penrose, Nuovo Cimento Riv. Ser. **1**, 252 (1969).
[24] D. Christodoulou, Phys. Rev. Lett. **25**, 1596 (1970).
[25] J. Levin and G. Perez-Giz, Phys. Rev. D **77**, 103005 (2008).
[26] J. Brink, M. Geyer, and T. Hinderer, Phys. Rev. D **91**, 083001 (2015).
[27] J. Levin and G. Perez-Giz, Phys. Rev. D **79**, 124013 (2009).
[28] G. Perez-Giz and J. Levin, Phys. Rev. D **79**, 124014 (2009).
[29] L. C. Stein and N. Warburton, Phys. Rev. D **101**, 064007 (2020).
[30] E. Hackmann and H. Xu, Phys. Rev. D **87**, 124030 (2013).
[31] J. Bicák and Z. Stuchlík, Mon. Not. R. Astron. Soc. **175**, 381 (1976).
[32] H. Goldstein, Z. Phys. **271**, 275 (1974).
[33] K. Glampedakis and D. Kennefick, Phys. Rev. D **66**, 044002 (2002).
[34] E. Stoghianidis and D. Tsoubelis, Gen. Relativ. Gravit. **19**, 1235 (1987).
[35] K. S. Thorne, Rev. Mod. Phys. **52**, 299 (1980).
[36] G. Magli, J. Math. Phys. (N.Y.) **36**, 5877 (1995).
[37] J. Bičák and T. Ledvinka, Phys. Rev. Lett. **71**, 1669 (1993).
[38] R. P. Kerr, Phys. Rev. Lett. **11**, 237 (1963).
[39] S. W. Hawking and G. F. R. Ellis, *The Large Scale Structure of Space-Time*, Vol. 1, Cambridge Monographs on Mathematical Physics (Cambridge University Press, Cambridge, England, 1973).
[40] I. Novikov and V. Frolov, *Physics of Black Holes*, Fundamental Theories of Physics Vol. 27 (Springer Science +Business Media, Berlin, 2013).
[41] R. H. Boyer and R. W. Lindquist, J. Math. Phys. (N.Y.) **8**, 265 (1967).
[42] Y. Hagihara, Jpn. J. Astron. Geophys. **8**, 67 (1930).
[43] A. Eleni and T. A. Apostolatos, Phys. Rev. D **101**, 044056 (2020).
[44] L. Euler, Mem. Berlin **16**, 228 (1760).
[45] L. Euler, Novi Commentarii Acad. Scient. Imperial. Petropolit. **10**, 152 (1764).
[46] G. Darboux, Arch. Neerl. Sci. Exactes Nat. **6**, 371 (1901).
[47] J. P. Vinti, J. Res. Natl. Bur. Stand. **63B**, 105 (1959).
[48] E. Aksenov, E. Grebennikov, and V. Demin, Artif. Earth Satell. (USSR) **8**, 64 (1961).
[49] D. Finkelstein, Phys. Rev. **110**, 965 (1958).
[50] F. de Felice and G. Preti, Classical Quantum Gravity **16**, 2929 (1999).
[51] L. P. Eisenhart, Ann. Math. **35**, 284 (1934).
[52] E. T. Whittaker, *A Treatise on the Analytical Dynamics of Particles and Rigid Bodies* (Cambridge University Press, Cambridge, England, 1937).
[53] E. Stoghianidis and D. Tsoubelis, Gen. Relativ. Gravit. **19**, 1235 (1987).